Floquet engineering of many-body states by the ponderomotive potential

Zhiyuan Sun [*]

Department of Physics, Tsinghua University, Beijing 100084, People's Republic of China
and Frontier Science Center for Quantum Information, Beijing 100084, People's Republic of China

The ponderomotive force is an effective static force that a particle feels in an oscillating field, whose static potential may be called the ponderomotive potential. We generalize this notion to periodically driven quantum many-body systems, and propose it as a convenient tool to engineer their nonequilibrium steady states beyond the single-particle level. Applied to materials driven by light, the ponderomotive potential is intimately related to the equilibrium optical conductivity, which is enhanced close to resonances. We show that the ponderomotive potential from the incident light may be used to induce exciton condensates in semiconductors, to generate attractive interactions leading to superconductivity in certain electron-phonon systems, and to create additional free-energy minima in systems with charge/spin/excitonic orders. These effects are presented with experimentally relevant parameters.

I. INTRODUCTION

There has been widespread interest in the nonequilibrium phenomena of many-body systems driven by a force that oscillates periodically in time [1–10]. A common example is solid-state materials driven by light in pump probe experiments [2,5,6,8,11–14]. This periodic drive can be viewed as a controlling knob that renders the materials in nonequilibrium steady states (NESS) that have properties absent in equilibrium, realizing "Floquet engineering" [4–6,10,14–19]. Floquet engineering of single-particle properties has been widely studied and well understood [4,11,12,14,19–24], while that of systems with many-body interactions has remained problematic [5,7–9,16,17,25–33].

The ponderomotive force [34–37] refers to the static second-order force $F_P = -\nabla[eE(r)]^2/(4m\omega^2)$ that a particle with charge e and mass m feels in an inhomogeneous electric field $\mathbf{E}(r)\cos(\omega t)$ oscillating at frequency ω. It originates from the particle's fast out-of-phase oscillation following the electrical force: When the fast force points to the direction of decreasing field, the particle locates closer to the strong field region, and vice versa, leading to a nonzero time average of the net force. One may define a ponderomotive potential by $F_P = -\nabla V_P(r)$ in the real-space coordinate r, as shown in Fig. 1. This notion is also the underlying physics for the Kapitza pendulum [38], and the optical lattices [39] and tweezers [40] that trap atoms and other objects. In this paper, we generalize the ponderomotive potential from $V_P(r)$ to $V_P(\phi)$ where ϕ means the generic degrees of freedom in periodically driven many-body systems, and show that it offers a convenient tool to engineer their NESS, as illustrated in Fig. 1.

II. PONDEROMOTIVE POTENTIAL

The Lagrangian of a generic periodically driven system may be written as

$$L = L_f[X, \phi] - 2f\cos(\omega t) \cdot P[X, \phi] + L_s[\phi] \qquad (1)$$

where X is the collection of the fast degrees of freedom, ϕ is the slow one, $f\cos(\omega t)$ is the periodic driving force with frequency ω, and $P(X, \phi)$ is the generalized polarization the force couples to. We assume that the driving term is slowly turned on, and that there is a bath (e.g., the phonons and the substrate) taking away any excessively generated heat so that the system is in a NESS. Note that in principle, the system should be described by a Keldysh path integral on the Keldysh time contour [1,41–44]. However, the physics could be understood qualitatively with the plain Lagrangian. For notational simplicity, we use Eq. (1) to represent the Keldysh action, and keep its full form in the appendices for curious readers.

The central goal of this paper is to integrate out X to obtain an effective Lagrangian or Hamiltonian for the slow field ϕ
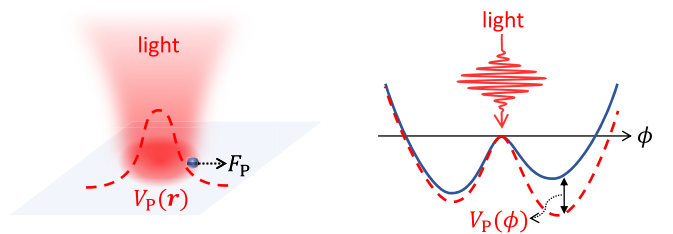

FIG. 1. (Left) An inhomogeneous optical field imposes the conventional ponderomotive potential $V_P(r)$ in real space for a particle. (Right) Uniform light imposes a generalized ponderomotive potential $V_P(\phi)$ for a collective degree of freedom ϕ in a many-body system. It modifies the energy landscape from the blue curve to the red-dashed one.

*Contact author: zysun@tsinghua.edu.cn

104301-1

with an energy cutoff ω, whose ground/thermal state is a good approximation to the NESS. This effective Lagrangian may be written as

$$L_P[\phi, f] = L_s[\phi] + V_0[\phi] + V_P(\phi, f), \quad F_P = -\partial_\phi V_P \quad (2)$$

where V_P is the static "ponderomotive potential" and F_P is the generalized ponderomotive force for the slow field ϕ, following the terminology for single particles. V_0 is the equilibrium term irrelevant to the drive. Note that the Lagrangian in our convention has a sign difference to the textbook one such that a lower potential means lower Lagrangian. We expand V_P in even powers of the driving force f,

$$V_P = \sum_{n=1}^{\infty} \chi^{(2n-1)}(\phi) f^{2n}. \quad (3)$$

If the driving term has multiple frequencies with components $f_1(\omega_1)$, $f_2(\omega_2)$,..., one just sums over all their products that combine to zero frequency. We start with a statement:

The coefficients in Eq. (3) are just the real parts of the retarded response functions of P to f at fixed ϕ in equilibrium:

$$\chi^{(1)}(\phi) = -\text{Re}[\chi_R(\phi; \omega)],$$
$$\chi^{(3)}(\phi) = -\text{Re}[\chi_R^{(3)}(\phi; \omega, -\omega, \omega)], ..., \quad (4)$$

in either of the following two cases: *Case 1:* There is no dissipation; *Case 2:* $L_f[X, \phi] = L_f[X]$, and P from Eq. (1) could be separated as $P_1(X)P_2(\phi)$.

Specifically, $\chi_R(\phi; \omega)$ is the linear response function of P to f at frequency ω, and $\chi_R^{(3)}(\phi; \omega, -\omega, \omega)$ is the third-order nonlinear response $[P(\omega)$ to $f(\omega)^2 f(-\omega)]$ [45]. For instance, if $L_f[X] = (-\dot{X}^2 + \omega_0^2 X^2)/2$ is that of a Harmonic oscillator and $P = X$, there is only linear response and $V_P = f^2/(\omega^2 - \omega_0^2)$. A simple interpretation is that the oscillator is polarized parallel (antiparallel) to the fast force f when $\omega < \omega_0$ ($\omega > \omega_0$), resulting in a negative (positive) coupling energy on average (the actual V_P is one half of this average coupling energy because of partial cancellation from L_f).

Case 1 (absence of dissipation) happens, for example, when the driving frequency is not equal to the intrinsic frequency of an ideal Harmonic oscillator, or when the frequency of an incident light is below the gap of an insulator (valid at the linear response level). In this case, the retarded response functions in Eq. (4) have no imaginary parts (away from poles), so that they are also equal to the advanced and time-ordered Green's functions [43,44]. Dissipation may arise from resonant excitation of the system by the drive, or from a bath [10,22,46–48] such that the spectrum of the system has nonzero line widths [49]. One could explicitly add the bath to Eq. (1) as a degree of freedom X_b that couples to X and ϕ. After integrating out the bath X_b, there are dissipation and fluctuation terms for X and ϕ captured by a Keldysh action [1,41–44,50,51]. Appendix A contains a proof of Eq. (4) by further integrating out the fast degree of freedom X using the Keldysh path integral.

For systems not covered by cases 1 and 2, one may compute the ponderomotive potential V_P case by case using Keldysh path integral and Green's functions, which are often simplified by classical approaches when quantum fluctuations are small. Classically, the force exerted on ϕ by the

fast degrees of freedom in Eq. (1) is $F_\phi = -\partial_\phi(L - L_s)$, and the ponderomotive force would simply be its time average, $F_P = \langle F_\phi \rangle_t$ (keeping only the terms dependent on the driving field f). In the absence of dissipation from a bath or from heat generation such that $X(t)$ is periodic in time and satisfies the Euler-Lagrange equation of motion, it is straightforward to show that the ponderomotive potential is simply the time averaged Lagrangian, $V_P = \langle L - L_s \rangle_t$. To compute its quantum mechanical version, one just replaces the time average by the path integral average, $F_P = \langle F_\phi \rangle_{\text{path integral}}$.

Compared to the high frequency Magnus expansion [16,25], which generates the effective static Hamiltonian by an expansion in the inverse driving frequency $1/\omega$, the ponderomotive potential in Eq. (3) is different in that it is an expansion in the driving field instead, which may be viewed as a resummation of the Magnus series. It does not require ω to be higher than all the energy scales of the system, such that Eq. (3) could capture the physics of dissipation [47] and resonances [8,52]. The ponderomotive potential may also be obtained from a Schrieffer-Wolff transformation [52] applied to the Lindblad master equation formulation of a driven dissipative system [represented by Eq. (1), or more rigorously, Eq. (A2)] that eliminates the periodic driving term order by order. However, the path integral approach applied here is convenient in separating the slow and fast fields and in making connections to response functions.

Materials driven by light

The most apparent real-world application of Eq. (3) is to materials driven by the dynamical electric field $2E\cos(\omega t)$ of light, which happens in, e.g., pump-probe experiments [2,5,6]. In this case, the response functions (polarizabilities) are simply related to the linear and nonlinear optical conductivities [35]. For example, the lowest-order term in Eq. (3) reads

$$V_P = \text{Re}\left[-\frac{i}{\omega}\sigma(\phi, \omega)\right]E^2 = \frac{1}{\omega}\sigma_2(\phi, \omega)E^2 \quad (5)$$

where $\sigma(\omega)$ is the optical conductivity of the system for fixed ϕ and σ_2 is its imaginary part. Similarly, the $n = 2$ term in Eq. (3) would be $\text{Re}[-i\sigma^{(3)}(\phi; \omega, -\omega, \omega)/\omega]E^4$ where $\sigma^{(3)}$ is the third-order optical conductivity [45,53], familiar to the nonlinear optics community. Since there are often peaks in $\sigma(\omega)$ from resonant transitions, V_P will be resonantly enhanced when the driving frequency is tuned close to these transitions.

If ϕ is the coordinate r of a single particle with charge e and mass m moving in an inhomogeneous optical field represented by $E(r)\cos(\omega t) = E_0 g(r)\cos(\omega t)$, the optical conductivity is just $\sigma = g(r)^2 ie^2/(m\omega)$, which plugged into Eq. (5) and Eq. (2) gives the static ponderomotive force $F_P = -\nabla[eE(r)]^2/(4m\omega^2)$ it experiences [34,35]. If the particle is an atom with an internal optical transition of energy ω_0 and linewidth γ, and X represents this internal degree of freedom, the ponderomotive potential from Eq. (5) is then $V_P \propto E(r)^2\text{Re}[1/(\omega^2 - \omega_0^2 + i\gamma\omega)]$. This is the potential that traps atoms in optical lattices and tweezers [39,40].

In Secs. III, IV, and V, we apply the ponderomotive potential to three examples to show that one may use it to engineer correlated states in materials driven by light.
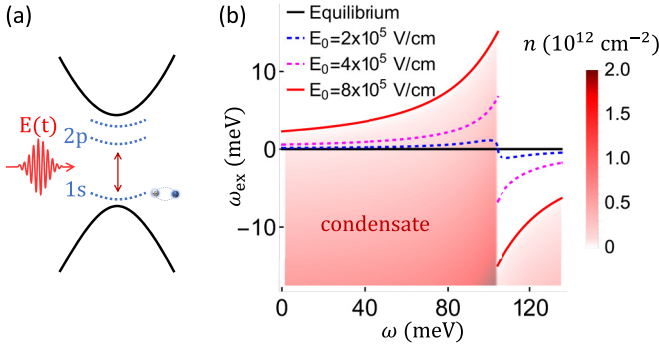
FIG. 2. (a) Schematics of the electron (black-solid curves) and exciton (blue-dashed curves) dispersion of a semiconductor and the pump light (red curve). (b) The phase diagram of the driven semiconductor on the plane of light frequency ω and the bare exciton energy. The curves are the boundaries between the semiconductor and condensate phases at different pumping electric fields E_0. The red color scale shows the exciton density of the condensate phase for $E_0 = 8 \times 10^5$ V/cm. The electron/hole mass is chosen as the vacuum electron mass $m = m_e$. The dielectric is $\epsilon = 7.0$, giving a Bohr radius of $a = 0.74$ nm and the $1s \to 2p$ transition energy $\omega_0 = 104$ meV. The damping rate is $\gamma = 8$ meV.

III. LIGHT-INDUCED EXCITON CONDENSATE

The first example is a semiconductor driven by coherent light at a subgap frequency ω. The exciton spectrum in the semiconductor is shown schematically in Fig. 2(a). Neglecting spatial fluctuations, the Lagrangian density for the lowest two excitons can be written as [54]

$$L = \Phi_s^*(-i\partial_t + \omega_{ex})\Phi_s + \Phi_p^*(-i\partial_t + \omega_p)\Phi_p + g\rho^2$$
$$+ \lambda E(t)(\Phi_p^*\Phi_s + \text{c.c.}) \qquad (6)$$

where Φ_s, ω_{ex} and Φ_p, ω_p are the bosonic fields and energies of the $1s$, $2p$ excitons, and g is the strength for the local interaction between the total density $\rho = \Phi_s^*\Phi_s + \Phi_p^*\Phi_p$. The dynamical electric field $E(t) = E_0 \cos(\omega t)$ interconverts the two excitons with the matrix element $\lambda = c_p ea$, where $c_p \sim 1$ and $a = \epsilon 2\hbar^2/(me^2)$ is the Bohr radius for the electron and hole with mass m and charge $\pm e$ bounded by Coulomb attraction screened by the dielectric ϵ. This coupling leads to the familiar $1s \to 2p$ optical transition in a Rydberg series. If the electric field is along the x direction, the Φ_p refers to the p_x exciton among the degenerate $2p$ excitons.

Without the driving term and for $\omega_{ex} > 0$, there are no excitons in the ground state. However, if the binding energy is large enough such that $\omega_{ex} < 0$, the s excitons spontaneously emerge and form an excitonic superfluid at low temperatures [54–56], as shown by the equilibrium phase boundary (black line) for the semiconductor-to-excitonic insulator transition in Fig. 2(b). For simplicity, we focus on the zero temperature case and the superfluid density is $\rho_0 = -\omega_{ex}/(2g)$ at the mean field level.

With the coherent light, we focus on its effect on the critical regime where ω_{ex} is close to zero, so that Φ_s is a slow field and Φ_p is the fast field to be integrated out. To be precise, the fast degree of freedom is the internal degree of freedom of an exciton responsible for the $1s$ to $2p$ transition, which

we use Φ_p to represent for notational simplicity. This system satisfies case 2 of Eq. (4) whether there is damping or not. Therefore, the $O(E^2)$ ponderomotive potential for the slow field is obtained from Eq. (5) as

$$V_P(\Phi_s) = \lambda^2 E_0^2 \text{Re}\left[\frac{\omega_0}{\omega^2 - \omega_0^2 + i\gamma\omega}\right]\Phi_s^*\Phi_s \qquad (7)$$

where $\omega_0 = \omega_p - \omega_{ex}$ is the transition energy and we have added a damping rate γ for the excitons. $V_P(\Phi_s)$ shifts down/up the effective energy of the $1s$ exciton if the driving frequency is red/blue tuned relative to the $1s \to 2p$ transition, whose effect is resonantly enhanced when ω is close to ω_0. Physically, compared to the optically silent state with no excitons, the state with a nonzero density of excitons has optical transitions with the optical conductivity σ_2 being negative at a red tuned frequency, giving a negative driving energy in Eq. (5), which favors such a state. As a result, the phase boundary of the nonequilibrium steady state is modified to the blue curve in Fig. 2(b). If ω_{ex} is just a little above zero, driving the system at a red tuned frequency obviously shifts the system from the semiconductor into the condensate phase, meaning "light-induced exciton condensate".

For stronger driving fields such that $\lambda E_0 \gtrsim |\omega - \omega_0|, \gamma$, the linear response becomes a poor approximation and one needs to sum all the terms in Eq. (3). Physically, the exciton undergoes oscillation between the $1s$ and $2p$ state where Φ_s has a fast component too. In this case, we write the excitonic field as $(\Phi_s, \Phi_p) = \Phi\xi$ so that $\Phi = \sqrt{\rho}e^{i\theta}$ is the total excitonic field, and the $1s$, $2p$ degree of freedom is viewed as the internal degree of freedom of the exciton encoded in the spinor $\xi = (\sqrt{1 - \eta}, \sqrt{\eta}e^{i\varphi})$. The Lagrangian in these variables becomes

$$L = \Phi^*(-i\partial_t + \omega_{ex})\Phi + g\rho^2 + \rho L_\xi,$$
$$L_\xi = \eta(\dot{\varphi} + \omega_0) + \lambda E(t)\sqrt{\eta(1 - \eta)}2\cos\varphi. \qquad (8)$$

L_ξ is just the Lagrangian of a pseudo spin $\mathbf{n} = \xi\sigma\xi^\dagger$ in the pseudo magnetic field $\mathbf{B} = (\lambda E(t), 0, \omega_0/2)$ where $\sigma = (\sigma_x, \sigma_y, \sigma_z)$ are the usual Pauli matrices.

Now the total exciton field Φ is the slow variable while the pseudo spin is the fast degree of freedom undergoing Rabi oscillation. If there is dissipation (formally introduced by the Keldysh action version of it), Eq. (8) is not covered by cases 1 and 2. Nevertheless, when there is a condensate such that the spin becomes classical, the ponderomotive force for Φ can be computed simply from $F_P = \Phi\langle -\partial_\rho(\rho L_\xi)\rangle_t$ where the time average is on the classical-dynamical orbit of the spin. The resulting ponderomotive potential predicts the pink and red lines as the phase boundaries for two strong driving fields in Fig. 2(b). A prominent feature is the discontinuity of the boundary as ω is tuned across the resonance, a consequence of the change of the stable orbit of the classical pseudospin. See Appendix B for details of the calculation.

Contrary to previously discussed mechanisms where the excitons are *generated* by light [57,58], this phenomenon does not require any interband optical matrix elements, but just the hydrogenic $s \to p$ optical matrix element of an exciton, which naturally exists. As one slowly turns on an optical field in a semiconductor, which does not have any optical transitions, the drive gradually lead the system into an exciton

condensate (which finally have optical transitions). Of course, the electrons and holes in the excitons must come from somewhere in this process, which could be the electrical contacts or small interband matrix elements in realistic devices. Therefore, this effect works for generic devices including those with interlayer excitons [58–60]. In devices made of GaAs [58] and transition metal dichalcogenides [59], the lowest-exciton energy is at the order of $\omega_{\text{ex}} \sim 1$ eV. To tune ω_{ex} to the energy range in Fig. 2, a practical method in the near term is to apply an electrical contact bias μ (to be distinguished from a huge gating field potentially causing dielectric breakdown) that shifts down the effective exciton energy to $\omega_{\text{ex}} - \mu$ [54,59].

This phenomenon may be partly understood as the optical Stark effect [61] where the s-exciton energy is pushed down in the Floquet picture for a red tuned driving frequency. However, the effective action approach in Eq. (2) is indispensable in determining the many-body steady state, especially when there is dissipation and a condensate.

IV. LIGHT-INDUCED SUPERCONDUCTIVITY

The second example is light-induced superconductivity in an electron-phonon system in a metal. It is described by the Lagrangian density

$$L = \tfrac{1}{2}\big[-\dot{X}^2 + \big(\omega_0^2 + g_e\rho\big)X^2\big] + E(t)X + L_e \quad (9)$$

where L_e is the electronic Lagrangian, and X represents an infrared (IR) active phonon, which couples linearly to the pump electric field $E(t) = 2E_0\cos(\omega t)$ but nonlinearly to the local electron density fluctuation $\rho(r)$ because of inversion symmetry [62–67].

Treating low-energy electrons as the slow field and X as the fast field, the ponderomotive potential for the electron density is found from Eq. (3) as

$$V_P(\rho) = \frac{E_0^2}{\omega^2 - \big(\omega_0^2 + g_e\rho\big)} \xrightarrow{O(\rho^2)} \frac{g_e^2 E_0^2}{\big(\omega^2 - \omega_0^2\big)^3}\rho^2. \quad (10)$$

Note that there are no higher-order terms in E_0 or quantum mechanical effects since a Harmonic oscillator has no nonlinear responses. The generated local density-density interaction is thus attractive/repulsive when ω is red/blue tuned relative to the phonon frequency ω_0, and experiences resonant enhancement when $\omega \approx \omega_0$, as shown by the black curve in Fig. 3. This explains previous results by Kennes *et al.* [62] and Sentef [63] and provides further insights.

When there is dissipation such that the phonon has a damping rate γ, the situation is not covered by case 1 or 2. By integrating out X in the Keldysh path integral (see Appendix C), the ponderomotive potential is obtained as

$$V_P = \frac{E_0^2}{\gamma\omega}\arctan\frac{\gamma\omega}{\omega^2 - \big(\omega_0^2 + g_e\rho\big)} \xrightarrow{O(\rho^2)} g_P\rho^2,$$

$$g_P = \frac{\omega^2 - \omega_0^2}{\big[\big(\omega^2 - \omega_0^2\big)^2 + \gamma^2\omega^2\big]^2}g_e^2 E_0^2. \quad (11)$$

Therefore, damping leads to broadening of this effect as shown in Fig. 3. Note that the branch of "arctan" should be selected such that V_P is continuous across the resonance.

Thanks to the exact quantum-classical correspondence in the response property of a Harmonic oscillator, Eq. (11) can
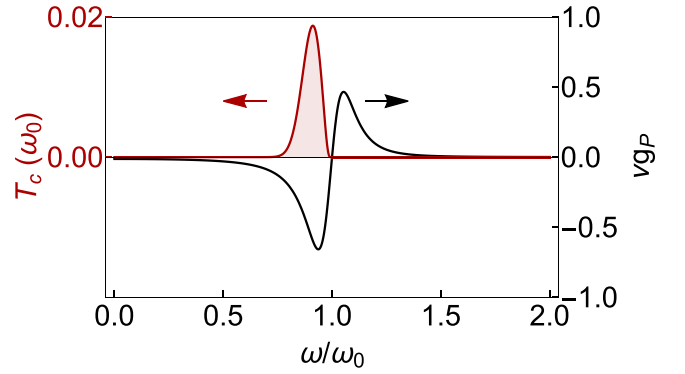

FIG. 3. The black curve is the dimensionless electron-electron interaction νg_P from Eq. (11) as a function of the light frequency ω for fixed driving electric field E_0. The red curve is the estimated superconducting T_c in units of ω_0. Plotted is for an infrared active phonon with the intrinsic frequency $\omega_0 = 10$ THz and the damping rate $\gamma = 2$ THz and other parameters specified in Appendix C 1 a.

also be derived from the classical equation of motion. The force for the electron density is just the square of the phonon displacement, $F_\rho = -\partial_\rho(L - L_e) = -g_e X^2/2$. Its time average gives the ponderomotive force $F_P = -g_e|\chi_R(\omega)|^2 E_0^2$ whose integral over ρ gives Eq. (11). Therefore, F_P pushes ρ in the direction that reduces the phonon frequency, so that the "driving energy" V_P [Eq. (10)] for a Harmonic oscillator goes down. Across the resonance, F_P has a peak rather than changing its sign as expected naively.

For a spherical Fermi surface, the dominant instability because of the attraction is towards the BCS superconductivity [68]. The resulting superconducting transition temperature $T_c \approx 1.13\Lambda e^{1/(\nu g_P)}$ for $g_P < 0$ is shown in Fig. 3, where the electronic density of states ν in the normal state and the other parameters are estimated in Appendix C 1 a for the fulleride K_3C_{60} [62], a possible system to test Eq. (11). The energy cutoff is chosen as $\Lambda = |\omega_0 - \omega|$ because g_P depends the frequency ω_e of ρ (to be distinguished from ω or ω_0) if one goes beyond the static ρ approximation in Eq. (11), whose behavior is expected to change for $\omega_e \gtrsim |\omega_0 - \omega|$ [69]. A detailed "strong coupling" calculation for T_c taking into account the ω_e dependence deserves future study.

To verify this effect in ultrafast experiments, one may use a multicycle pump pulse with a bandwidth smaller than the linewidth of the IR phonon, and measure the transient state (similar to recent experiments [70,71] but with relatively well defined pump frequencies close to the relevant IR phonon, and with a probe pulse overlapping with the pump instead of after the pump is gone). An interesting prediction of Fig. 3 is that superconductivity is enhanced/suppressed if the pump frequency ω is lower/higher than the IR phonon frequency ω_0. If the equilibrium state is already superconducting, the pump would lead to a Fano-like asymmetric lineshape of T_c as ω is scanned across ω_0. Possible systems include K_3C_{60} [70] and doped $SrTiO_3$ [72]. See Appendix C 1 b for estimates of heating.

A different scenario is the state after a short pump pulse, when the IR phonon oscillates freely with an amplitude X_0 [62,70]. If the electron density varies slowly, the oscillation amplitude changes adiabatically with the action

$S \propto \sqrt{\omega_0^2 + g_e \rho} X_0(\rho)^2$ (the adiabatic invariant) kept constant. Therefore, the ponderomotive force is $F_P(\rho) = -\langle g_e X^2/2 \rangle_t = -g_e X_0(\rho)^2/4 = -\frac{1}{4} X_0(0)^2 |\omega_0| / \sqrt{\omega_0^2 + g_e \rho}$, rendering the potential $V_P = \frac{1}{2} |\omega_0| / \sqrt{\omega_0^2 + g_e \rho} X_0(0)^2$, generalizing the result of Kennes *et al.* [62]. At order ρ^2, the density-density interaction strength $g_P = -X_0(0)^2/(16\omega_0^2)$ is always negative. Since the excitation efficiency of the IR phonon by the pump has a peak at its resonance, it is consistent with a recent experiment on $K_3 C_{60}$ [70]. Nevertheless, this explanation serves only as a possibility of what happened in $K_3 C_{60}$ [70,73–75], among other mechanisms such as the one involving Jahn-Teller Hg phonons [76]. The actual mechanism for the light-induced superconducting-like state requires more involved study, especially considering its metastability [76,77].

The ponderomotive potential also provides a simple derivation for the light enhanced electron-electron attraction in a Raman phonon model [78,79]; see Appendix C 2.

V. LIGHT-ENGINEERED FREE-ENERGY LANDSCAPE

The third example is light-induced new free-energy minima in systems with excitonic order (excitonic insulator [80]) or charge/spin density wave (CDW/SDW) order [81,82] because of Fermi surface nesting in the BCS weak coupling case. The Lagrangian density [83,84] is

$$L = \psi^\dagger \begin{pmatrix} -i\partial_t + \xi(p) & \Delta \\ \Delta^* & -i\partial_t - \xi(p) \end{pmatrix} \psi + \frac{1}{g} |\Delta|^2 \quad (12)$$

where $p = -i\nabla + A(t)$, $A(t) = 2A_0 \cos \omega t$ is the vector potential of the coherent light, g is the coupling constant, and $\psi = (\psi_1, \psi_2)^T$ is the two-component fermion field for two electronic bands with energy $\xi(p)/-\xi(p)$. They correspond to the overlapping conduction and valence bands [$\xi(p) = p^2/(2m) - \mu$] in the case of excitonic order, and the left and right moving bands [$\xi(p) = v_F p$] nested together by twice the Fermi wave vector in the case of charge/spin order where v_F is the Fermi velocity. The complex order parameter Δ leads to a quasiparticle gap.

We treat Δ as the slow field and ψ as the fast one. If $\omega < 2\Delta$ and there is no bath such that there is no dissipation, Eq. (12) satisfies case 1 of Eq. (4) so that Eq. (5) gives the ponderomotive potential

$$V_P(\Delta) = \frac{E_0^2}{\omega^2} \frac{n}{m} \left(1 - \frac{2\Delta}{\omega} \frac{\sin^{-1}\left(\frac{\omega}{2\Delta}\right)}{\sqrt{1 - \left(\frac{\omega}{2\Delta}\right)^2}} \right) \quad (13)$$

at order E_0^2, where $E_0 = \omega A_0$ is the amplitude of the driving electric field and n, m are the density of carriers in the normal state and their effective mass, and we have set the elementary charge to be unity. The optical conductivity σ at zero temperature is taken from Eq. (12) of Ref. [84] neglecting the BaSh mode. Since V_P is negative for $2\Delta > \omega$ and diverges as $-1/\sqrt{\delta}$ as the detuning $\delta = 2\Delta - \omega$ approaches zero (a result of the interband transitions at $\omega > 2\Delta$), it tends to push Δ to smaller values.

Note that for $U(1)$ invariant CDW/SDW systems, unlike excitonic insulators, the gapless phase mode shifts the
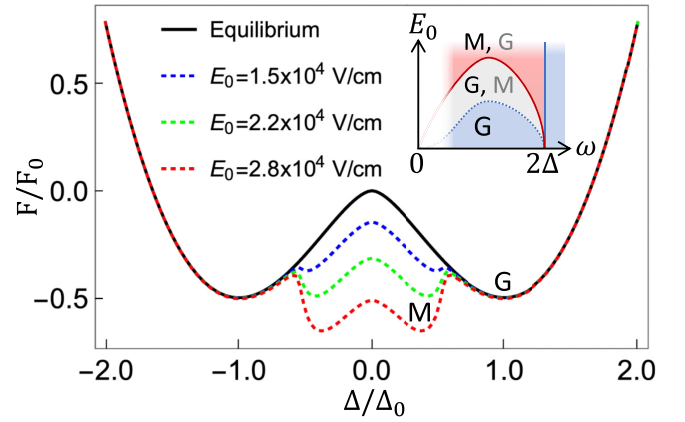

FIG. 4. The effective free energy for a system with charge/spin/excitonic order driven by light at several field strengthens E_0 for $\omega = 30$ THz and $\gamma = 1$ THz. The gap at equilibrium is $2\Delta_0 = 55$ THz, at the same order as that in $Ta_2 NiSe_5$ [85]. The order parameter Δ and the free energy F are in units of Δ_0 and $F_0 = \nu \Delta_0^2$. The top-right inset is a schematic phase diagram on the plane of driving frequency ω and field strength E_0. Black symbol means the global minimum while gray symbol means a metastable minimum. The white region is beyond the validity of the analytical formula in this paper.

optical absorption from quasiparticle excitations to zero frequency [81,82]. However, this effect is absent in most materials because of strong pinning by the lattice and disorder [81,82], such that the optical conductivity used in Eq. (13) still holds.

To study the case of $\omega > 2\Delta$ when there is absorption, one needs a bath that takes away the heat, which is implicitly treated as a damping rate γ of the quasiparticles. The system is no longer covered by cases 1 or 2, and one must compute V_P by explicitly integrating out ψ in the Keldysh action, giving a lengthy expression for the ponderomotive force $F_P(\Delta)$, as in Appendix D. It corrects the effective free energy to

$$F = -\nu |\Delta|^2 \ln \frac{\Lambda}{|\Delta|} + \frac{1}{g} |\Delta|^2 + V_P(\Delta) \quad (14)$$

at zero temperature where Λ is the energy cutoff.

The landscape $F(\Delta)$ is plotted in Fig. 4 for several driving electric fields. Being negative, F_P always pushes Δ to smaller values. Notably, the quasiparticle excitation peak at $\Delta \lesssim \omega/2$ contributes a "dissipative peak" in F_P that scales inversely with γ. Physically, each Anderson pseudo spin σ (in the diagonalized band basis) close to the gap edge contributes a force $\propto \sigma_z$ for Δ. Resonant optical excitation reduces σ_z by an amount $\propto E_0^2/\gamma^2$, contributing a negative ponderomotive force on top of the equilibrium force. This force leads to the abrupt drop of the potential around $\Delta = \omega/2$ in Fig. 4, which creates a new minimum labeled by "M" for strong enough fields. As the light intensity grows further, the energy of this minimum goes below that of the original minimum "G", and the system undergoes a first-order phase transition from G to M, as shown by the red solid curve in the schematic nonequilibrium phase diagram in the inset of Fig. 4. In an ultrafast experiment, one could measure the quasiparticle gap by a probe pulse overlapping with a multicycle pump pulse. The nonequilibrium phase

transition would manifest as a sharp drop of the gap as the pump fluence is increased beyond the threshold.

VI. DISCUSSION

We have introduced the ponderomotive potential by Eqs. (1)–(3) to study periodically driven many-body systems. We proved its intimate relation to the equilibrium response functions in Eq. (4), which in the context of materials driven by light are shown to be the familiar linear [Eq. (5)] and nonlinear optical conductivities, offering a quick and convenient way to obtain physical insights. We also applied it to three realistic examples and found interesting light-induced states to be verified by experiments. With this concept, we anticipate more exotic nonequilibrium steady states to be discovered, especially in systems with a manifold of (nearly) degenerate low-energy states [29,30,54] such that even a weak drive could seamlessly engineer the energy landscape.

Although we assumed a bath that takes away the heat such that the NESS exists, the ponderomotive potential may also apply to the quasisteady states in the prethermal stage of driven isolated systems [7,25–27]. In conclusion, we expect the ponderomotive potential to be a convenient tool for studying the nonequilibrium phenomena in driven systems. To go beyond it, one may look for nonconservative ponderomotive forces, or could perform systematic expansions to include the Kinetic terms in the effective low-energy Lagrangian.

APPENDIX A: PROOF OF Eq. (4)

It may look natural that the coefficients in Eq. (3) are roughly the response functions if one "integrates out" the fast degree of freedom X assuming fixed ϕ. However, since one is dealing with the nonequilibrium case of periodically driven systems, this integrating out procedure has to be done by the real-time path integral, for which a natural framework is the path integral on the Keldysh time contour [1,41–44]. In the Keldysh path integral [43,44], one defines a generating functional, the "partition function", as

$$Z[f(s)] = \text{Tr}[\hat{U}(s)\hat{\rho}] = \int_C D[X(s), \phi(s)]e^{-iS[X,\phi,f]} = \int D[X_c, X_q; \phi_c, \phi_q]e^{-iS[X_c, X_q; \phi_c, \phi_q; f]} \tag{A1}$$

on the closed time contour C parameterized by s, which runs from time $t = 0$ to time $t = t_f$ (forward contour) and then from time $t = t_f$ to time $t = 0$ (backward contour). Here $\hat{\rho}$ is the initial density matrix of the system at time zero, $X_{c/q}(t) = (X_+ \pm X_-)/\sqrt{2}$ is the "classical"/"quantum" component of the fast field X following the Keldysh notation, and $X_+(t)$ and $X_-(t)$ are their values on the forward and backward time contours. Notations for ϕ and other symbols are defined in the same way. Without the external field $f(s)$, one have $Z = 1$. However, $Z \neq 1$ if $f(s)$ has different values on the forward and backward time contours so that the path integrals on the two contours do not cancel each other, or in other words, $\hat{U}(s) \neq \hat{I}$. The functional dependence of Z on $f(s)$ contains the information of observables, correlation functions, etc.

The Keldysh action for a generic periodically driven system [Eq. (1)] is

$$S = S_f[X_c, X_q; \phi_c, \phi_q] + S_s[\phi_c, \phi_q] + \int dt\, f(t)(P[X_+, \phi_+] - P[X_-, \phi_-]), \quad f(t) = 2f\cos(\omega t). \tag{A2}$$

Equation (A2) is, in general, the action after integrating out any degrees of freedom from the bath. Further integrating out the fast degree of freedom X in Eq. (A1), one obtains the effective action for ϕ,

$$S[\phi_c, \phi_q; f] = S_s[\phi_c, \phi_q] + S_P[\phi_c, \phi_q; f], \quad S_P = -\int dt\, \phi_q F_P(\phi_c, f) + O(\phi_q^2). \tag{A3}$$

From the construction of the Keldysh action, the coefficient of the $O(\phi_q)$ term is the derivative of the potential for ϕ. Therefore, $F_P(\phi_c, f)$ is the ponderomotive force and $V_P(\phi_c, f) = -\int d\phi_c F_P(\phi_c, f)$ is the ponderomotive potential. In the following, we prove Eq. (4) for the two cases stated there.

1. Response functions

In this subsection, we define the linear and nonlinear response functions of the generalized polarization P to the generalized force $f(t)$ in Eq. (A2) [43,44]. We allow the force (source field) $f(s)$ to have different values $f_+(t)$, $f_-(t)$ on the two contours and define $f_c(t)$ and $f_q(t)$ in the same way as the fields X and ϕ, so that the coupling term in Eq. (A2) generalizes to $f_c P_q + f_q P_c$ where $P_{c,q} = (P[X_+, \phi_+] \pm P[X_-, \phi_-])\sqrt{2}$. The physical external field has $f_c(t)$ only, while $f_q(t)$ is introduced for convenience. The physical polarization is found from the generating functional $Z = e^{-iS[f_c, f_q]}$ as

$$P_c(t) = -i\frac{\delta Z[f_c, f_q]}{\delta f_q(t)}\bigg|_{f_q=0} = \sum_{m=1}^{\infty} \int dt_1 dt_2...dt_m \frac{1}{m!}\chi_r^{(m)}(t; t_1, t_2, ..., t_m) \cdot f_c(t_1)f_c(t_2)...f_c(t_m). \tag{A4}$$

Here

$$\chi_{\mathrm{r}}^{(m)}(t;t_1,t_2,...,t_m) \equiv -i\frac{\delta Z[f_c,f_q]}{\delta f_q(t)\delta f_c(t_1)\delta f_c(t_2)...\delta f_c(t_m)}\Bigg|_{f_{c,q}=0} = \langle P_c(t)P_q(t_1)P_q(t_2)...P_q(t_3)\rangle \tag{A5}$$

is defined as the mth order symmetrized retarded response function and $\langle...\rangle$ means the correlation function under the Keldysh path integral at $f_{c,q} = 0$ in Eq. (A1). Therefore, the effective action for f could be written as

$$S[f_c,f_q] = -\sum_{m=1}^{\infty}\int dt_1 dt_2...dt_m \frac{1}{m!}\chi_{\mathrm{r}}^{(m)}(t;t_1,t_2,...,t_m)\cdot f_q(t)f_c(t_1)f_c(t_2)...f_c(t_m). \tag{A6}$$

at order f_q. If the source field is a single frequency one, meaning $f_{c/q}(t) = 2f_{c/q}\cos(\omega t)$, the effective action contains the products of f whose frequencies sum to zero. This occurs for odd $m = 2n-1$ only,

$$S[f_c,f_q] = -\sum_{n=1}^{\infty}\frac{C_{2n}^n}{(2n-1)!}\chi_{\mathrm{r}}^{(2n-1)}(\omega,-\omega,\omega,...)\cdot f_q f_c^{2n-1}, \quad \chi_R^{(2n-1)} \equiv \frac{1}{(n!)^2}\chi_{\mathrm{r}}^{(2n-1)} \tag{A7}$$

where $\chi_R^{(2n-1)}(\omega,-\omega,\omega,...)$ is the response function (A5) in the frequency representation, and the C_{2n}^n factor comes from the different ways of assigning the n positive frequencies (ω) and n positive frequencies ($-\omega$) to $f_{c/q}$. We have also defined the new response function $\chi_R^{(2n-1)}$ in Eq. (A7) for notational simplicity of the main text.

2. Case 1

Since there is no dissipation, there is no bath that is integrated out, so that the system is an isolated system. Therefore, the fields on the forward and backward time contours are not coupled [43,44], meaning the action in Eq. (A2) could be written as $S = S_+ - S_-$ where

$$S_+ = \int dt L[X_+,\phi_+,f_+], \quad S_- = \int dt L[X_-,\phi_-,f_-], \quad L = L_f[X,\phi] + L_s[\phi] + 2f\cos(\omega t)\cdot P[X,\phi] \tag{A8}$$

and $f_+ = f_- = f$. However, we have given different labels to f on the two contours for later convenience. To derive the F_{P} in Eq. (A3), one just needs to assume constant ϕ_+ and ϕ_- on the two contours. Because we assume that the NESS exists, the path integral on each contour is a product of infinite periods T, which may or may not be $2\pi/\omega$. In the limit of $t_f \to \infty$, the boundary conditions at $t = 0$ and $t = t_f$ that glue the actions on the two contours will not be important, so that the two path integrals over X on the two contours are decoupled from each other. Therefore, after integrating out X, one has $S = S_+ - S_-$ where

$$S_+ = \sum_{n=1}^{\infty}\chi^{(2n-1)}(\phi_+)f_+^{2n}, \quad S_- = \sum_{n=1}^{\infty}\chi^{(2n-1)}(\phi_-)f_-^{2n}. \tag{A9}$$

For $\phi_+ = \phi_- = \phi$ in Eq. (A9), one has

$$S = S_+ - S_- = \sum_{n=1}^{\infty}\chi^{(2n-1)}(\phi)(f_+^{2n} - f_-^{2n}) = \sum_{n=1}^{\infty}\chi^{(2n-1)}(\phi)\big(2nf_q f_c^{(2n-1)} + O(f_q^3)\big). \tag{A10}$$

Since the coefficient of the $O(f_q)$ term should be the retarded response functions, comparing with Eq. (A7) leads to $\chi^{(2n-1)}(\phi) = -\chi_R^{(2n-1)}(\phi)$. Now, setting $f_+ = f_- = f$ in Eq. (A9), one has

$$S = S_+ - S_- = \sum_{n=1}^{\infty}\big(\phi_q\partial_{\phi_c}\chi^{(2n-1)}(\phi_c) + O(\phi_q^3)\big)f^{2n}. \tag{A11}$$

The above two equations combined with Eq. (A3) lead to the conclusion that the ponderomotive force is $F_{\mathrm{P}}(\phi_c) = \sum_n \partial_{\phi_c}\chi_R^{(2n-1)}(\phi_c)f^{2n}$ and the ponderomotive potential is $V_{\mathrm{P}}(\phi_c) = -\sum_n \chi_R^{(2n-1)}(\phi_c)f^{2n}$.

3. Case 2

Case 2 can incorporate any bath (integrated out) and dissipation in Eq. (A2). However, it requires $S_f = S_f[X_c,X_q]$ such that the "fast" action for X is not affected by ϕ. It also requires that the generalized polarization P could be separated as a product $P_1(X)P_2(\phi)$ in Eq. (1). Up to the linear order in ϕ_q, the coupling Lagrangian in Eq. (A2) could be written as

$$L_c = 2f\cos(\omega t)\cdot[P_q(X_c,X_q,\phi_c) + \phi_q\partial_{\phi_c}P_c(X_c,X_q,\phi_c)],$$
$$P_c = P[X_c+X_q,\phi_c] + P[X_c-X_q,\phi_c], \quad P_q = P[X_c+X_q,\phi_c] - P[X_c-X_q,\phi_c], \tag{A12}$$

where P_c and P_q are the "classical" and "quantum" components of the generalized polarization. From Eq. (A3), after integrating out X, the ponderomotive force for ϕ_c is therefore

$$F_{\mathrm{P}}(\phi_c) = \sum_{n=1}^{\infty} \frac{C_{2n}^n}{(2n-1)!} C^{(2n)}(\phi_c) f^{2n}, \quad C^{(2)}(\phi_c) = \langle P_q \partial_{\phi_c} P_c \rangle|_{(\omega, -\omega)}, \quad C^{(4)}(\phi_c) = \langle P_q P_q P_q \partial_{\phi_c} P_c \rangle|_{(\omega, -\omega, \omega, -\omega)}, ..., \quad \text{(A13)}$$

where $\langle \rangle$ means the correlation function: functional average over $X_c(t)$, $X_q(t)$ using the Keldysh path integral in Eq. (A1) at $\phi_q = 0$ and fixed ϕ_c. Since $P = P_1(X)P_2(\phi)$ is separable, one has $P_c = P_{1c}P_2(\phi_c)$ and $P_q = P_{1q}P_2(\phi_c)$ where $P_{1c/q} = (P_1[X_+] \pm P_1[X_-])/\sqrt{2}$. Therefore, for constant ϕ, the coefficients can be written as

$$C^{(2)}(\phi_c) = \tfrac{1}{2}\partial_{\phi_c}\langle P_q P_c \rangle|_{(\omega,-\omega)} = \tfrac{1}{2}\partial_{\phi_c}\chi_r(\omega,-\omega), \quad C^{(4)}(\phi_c) = \tfrac{1}{4}\partial_{\phi_c}\langle P_q P_q P_q P_c \rangle|_{(\omega,-\omega,\omega,-\omega)} = \tfrac{1}{4}\partial_{\phi_c}\chi_r^{(3)}|_{(\omega,-\omega,\omega,-\omega)}, ..., \quad \text{(A14)}$$

By comparison with Eq. (A7), one concludes that $F_{\mathrm{P}}(\phi_c) = \sum_n \partial_{\phi_c} \chi_R^{(2n-1)}(\phi_c) f^{2n}$. Making use of the symmetric properties of the real parts of response functions, one obtains Eq. (4).

APPENDIX B: LIGHT-INDUCED EXCITON CONDENSATE

For the reader's convenience, we reproduce the Lagrangian [Eq. (8)] of the excitons here,

$$L = L_s[\Phi] + \rho L_\xi, \quad L_s[\Phi] = \Phi^*(-i\partial_t + \omega_{\mathrm{ex}})\Phi + g\rho^2, \quad L_\xi = \eta(\dot\varphi + \omega_0) + \lambda E(t)\sqrt{\eta(1-\eta)}2\cos\varphi. \quad \text{(B1)}$$

Writing the internal degree of freedom ϕ, η as a pseudovector on the unit sphere,

$$\mathbf{n} = \xi\sigma\xi^\dagger = (2\sqrt{\eta(1-\eta)}\cos\varphi, \; -2\sqrt{\eta(1-\eta)}\sin\varphi, \; 1-2\eta), \quad \text{(B2)}$$

L_ξ could also be written as

$$L_\xi = -\mathbf{A}(\mathbf{n})\cdot\dot{\mathbf{n}} - \mathbf{B}(t)\cdot\mathbf{n} + B_z, \quad (B_x, B_y, B_z) = \left(\lambda E(t), \; 0, \; \frac{\omega_0}{2}\right) \quad \text{(B3)}$$

where $\mathbf{B}$ is the effective "magnetic field" and $\mathbf{A}(\mathbf{n})$ is the Berry connection on the unit sphere for the spin coherent state path integral. The corresponding Berry curvature is $\mathbf{\Omega}(\mathbf{n}) = d\mathbf{A}(\mathbf{n}) = \mathbf{n}/2$. After adding the dissipative terms, one may write down the Keldysh version of Eq. (B1),

$$L = L_s[\Phi_c, \Phi_q] + L_f[\Phi_c, \Phi_q, \mathbf{n}_c, \mathbf{n}_q],$$
$$L_f = \Phi_c^*\Phi_c\mathbf{n}_q \cdot [-\dot{\mathbf{n}}_c \times \mathbf{\Omega}(\mathbf{n}_c) - \mathbf{B}(t) + \gamma\dot{\mathbf{n}}_c] + [\Phi_q^*\Phi_c[-\dot{\mathbf{n}}_c\mathbf{A}(\mathbf{n}_c) - \mathbf{B}(t)\mathbf{n}_c + B_z] + \mathrm{c.c.}. \quad \text{(B4)}$$

The classical saddle point $\partial_{\mathbf{n}_q} L = 0$ for the spin (together with the constraint that $|\mathbf{n}| = 1$) is just the Landau–Lifshitz–Gilbert equation for a classical magnet,

$$\dot{\mathbf{n}}_c = 2\mathbf{n}_c \times (-\mathbf{B}(t) + \gamma\dot{\mathbf{n}}_c). \quad \text{(B5)}$$

It is has the interpretation of a massless particle moving on the unit sphere under the magnetic field $\mathbf{\Omega}(\mathbf{n}_c)$ and in the potential $-\mathbf{B} \cdot \mathbf{n}_c$, and experiencing the friction $-\gamma\dot{\mathbf{n}}_c$.

1. Stable orbit of the driven classical spin

To compute the ponderomotive force for Φ, one needs to solve for the stable classical orbit of $\mathbf{n}_c$ from Eq. (B5), for which a general analytical solution is unknown. Fortunately, since we aim at the resonance regime $|\omega - \omega_0| \lesssim \lambda E_0$ to obtain the higher-order corrections to the $O(E_0^2)$ result, it is reasonable to make the rotating wave approximation,

$$(B_x, B_y, B_z) = \left(\lambda E_0 \cos(\omega t), \; \frac{\omega_0}{2}\right) \to (B_\perp \cos(\omega t), \; B_\perp \sin(\omega t), \; B_z), \quad B_\perp = \frac{\lambda E_0}{2}, \quad B_z = \frac{\omega_0}{2}. \quad \text{(B6)}$$

Now the drive is an effective magnetic field $B_\perp$ rotating on the $x - y$ plane with angular frequency ω. The stable orbit should be the unit vector $\mathbf{n}_c(t) = (\sin\theta_0\cos(\omega t + \varphi_0), \; \sin\theta_0\sin(\omega t + \varphi_0), \; \cos\theta_0)$ rotating at the same angular frequency. In the rotating frame, it is a stable point $\mathbf{n}_c = (n_x, n_y, n_z) = (\sin\theta_0\cos\varphi_0, \; \sin\theta_0\sin\varphi_0, \; \cos\theta_0)$. Plugging it into Eq. (B5) yields the equation for the angles,

$$-\delta\sin\theta_0 - B_\perp\cos\theta_0\cos\varphi_0 = 0, \quad \tfrac{1}{2}\gamma\omega\sin\theta_0 + B_\perp\sin\varphi_0 = 0, \quad \text{(B7)}$$

where $\delta = (\omega - \omega_0)/2$ is the detuning. The solution is

$$n_z^2 = 1 - \frac{1}{2}\left[1 + \frac{1}{\gamma^2\omega^2/4}(\delta^2 + B_\perp^2) \pm \sqrt{\left(1 + \frac{1}{\gamma^2\omega^2/4}(\delta^2 + B_\perp^2)\right)^2 - 4\frac{B_\perp^2}{\gamma^2\omega^2/4}}\right], \quad \sin\varphi_0 = -\frac{\gamma\omega/2}{B_\perp}\sin\theta_0. \quad \text{(B8)}$$

Note that for each field $B_\perp$ and driving frequency ω, there is a pair of solutions to Eq. (B8), i.e., (θ_0, φ_0) and $(\pi - \theta_0, \pi - \varphi_0)$. These two points as functions of the driving frequency ω correspond to the solid and dashed curves in Fig. 5. However, only the
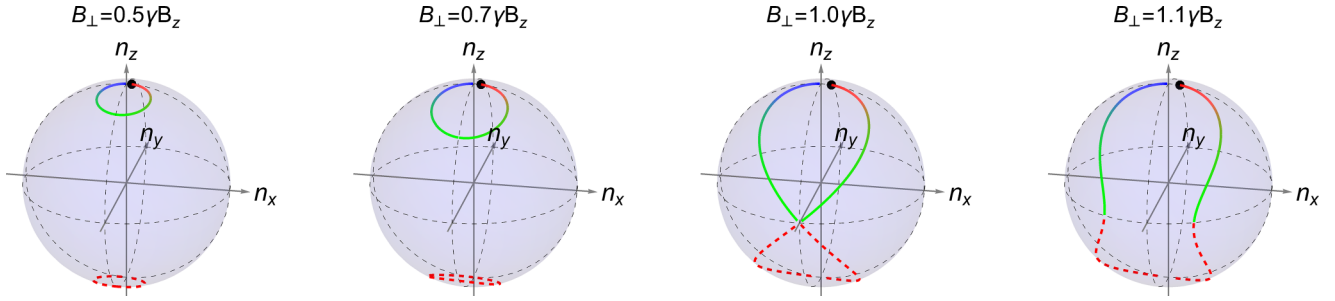
FIG. 5. Solid curves are the stable stationary $\mathbf{n}_c = (\sin\theta_0 \cos\varphi_0,\ \sin\theta_0 \sin\varphi_0,\ \cos\theta_0)$ of the driven dissipative classical spin in the rotating frame as a function of the driving frequency ω. On these curves, red means $\omega = 0$, green means $\omega = \omega_0$, blue means $\omega = \infty$, and other values of frequency interpolates among these colors. The black dots are the stable points at $\omega = 0$. The red-dashed curves are the corresponding unstable stationary points. The four panels are for different values of the driving field $B_\perp = \lambda E_0/2$. The dimensionless damping rate is $\gamma = 0.1$. Beyond the critical driving field, $B_\perp = \gamma B_z > \gamma\omega_0/2$, the curve becomes disconnected, meaning that there is a jump of $\mathbf{n}_c$ as the driving frequency ω crosses ω_0.

point on the north hemisphere (solid curves) is the stable one, while that on the south hemisphere (dashed curves) is unstable, which would relax to the former location because of fluctuations. From the perspective of continuity, as the driving field increases gradually from zero to beyond the critical one, the solid curve continuously expands from the circle in the left panels to the disconnected curves in the right panel.

2. The ponderomotive potential

We now compute the ponderomotive force $F_{\mathrm{P}}(\Phi_c) = \lim_{T\to\infty}\langle\frac{1}{T}\int_0^T dt\,\partial_{\Phi_q^*}L_f\rangle$ for Φ at the mean-field level. This means we approximate the path integral average $\langle\rangle$ by the classical saddle point from the previous section,

$$F_{\mathrm{P}}(\Phi_c) = -\langle\partial_{\Phi_q^*}L_f\rangle_t = -\Phi_c\langle[-\dot{\mathbf{n}}_c\mathbf{A}(\mathbf{n}_c) - \mathbf{B}(t)\mathbf{n}_c + B_z]\rangle_t. \tag{B9}$$

Plugging the stable orbit of Eq. (B8) into Eq. (B9) yields the ponderomotive force, and the ponderomotive potential

$$V_{\mathrm{P}}(\Phi) = |\Phi|^2\langle[-\dot{\mathbf{n}}_c\mathbf{A}(\mathbf{n}_c) - \mathbf{B}(t)\mathbf{n}_c + B_z]\rangle_t = |\Phi|^2[(B_z - \omega/2)(1 - n_z) - B_\perp n_x] \tag{B10}$$

used for Fig. 2. At the resonant $\omega \to \omega_0$, one has

$$(n_x,\ n_z,\ V_{\mathrm{P}}) = \begin{cases} \left(0,\ \sqrt{1 - \frac{B_\perp^2}{\gamma^2 B_z^2}},\ 0\right), & B_\perp \leqslant \gamma B_z \\[3mm] \left(\sqrt{1 - \frac{\gamma^2 B_z^2}{B_\perp^2}},\ 1,\ -|\Phi|^2 B_\perp\sqrt{1 - \frac{\gamma^2 B_z^2}{B_\perp^2}}\right), & B_\perp > \gamma B_z\ \&\ \omega = \omega_{0-} \\[3mm] \left(-\sqrt{1 - \frac{\gamma^2 B_z^2}{B_\perp^2}},\ 1,\ -|\Phi|^2 B_\perp\sqrt{1 - \frac{\gamma^2 B_z^2}{B_\perp^2}}\right), & B_\perp > \gamma B_z\ \&\ \omega = \omega_{0+} \end{cases} \tag{B11}$$

where $B_\perp = \lambda E_0/2 = c_p a_0 e E_0$ is the energy scale of the field strength. For a dielectric screening of $\epsilon = 7.0$, one obtains the Bohr radius $a_0 = 0.74$ nm, the $s \to p$ transition energy $\omega_0 = 104$ meV and the shape factor $c_p = 0.53$. These parameters give $B_\perp = 2$ meV for an electric field of $E_0 = 10^5$ V/cm. Figure 2 is based on these parameters.

APPENDIX C: LIGHT-ENHANCED ELECTRON-ELECTRON ATTRACTION

1. The infrared phonon model

In this section, we consider the infrared phonon coupled to a general inversion-even electronic degree of freedom ϕ,

$$L = \tfrac{1}{2}\big[-\dot{X}^2 + \big(\omega_0^2 + \phi\big)X^2\big] + E(t)X. \tag{C1}$$

Note that ϕ is in general a functional of electronic degrees of freedom, which may also contain time derivatives, and reduces to $\phi = g_e\rho$ in the simple case discussed in Sec. IV. After adding the damping rate γ of the phonon, the Keldysh version [43,44] of the Lagrangian is written as

$$L = \frac{1}{2}(X_c\ \ X_q)\begin{pmatrix} \phi_q & \partial_t^2 + \gamma\,\partial_t + \omega_0^2 + \phi_c \\ \partial_t^2 - \gamma\,\partial_t + \omega_0^2 + \phi_c & -2\gamma\,\partial_t\coth\frac{i\partial_t}{2T} + \phi_q \end{pmatrix}\begin{pmatrix} X_c \\ X_q \end{pmatrix} + E(t)X_q \tag{C2}$$

to linear order in ϕ_q, where T is the temperature of the bath. Integrating out X and looking for the $O(\phi_q)$ term according to Eq. (A1), one obtains the exact ponderomotive force for ϕ,

$$F_P = -\frac{1}{2}\langle X^2 \rangle = -\frac{1}{2}\left(X_0^2 + X_{\text{driven}}^2\right) = F_0 + \chi_R(\phi_c,\omega)\chi_A(\phi_c,\omega)E_0^2, \quad \chi_R(\phi_c,\omega) = \frac{1}{-\omega^2 - i\gamma\omega + \omega_0^2 + \phi_c}, \quad \chi_A = \chi_R^* \quad \text{(C3)}$$

where χ_R and χ_A are the retarded and advanced response functions of the IR phonon.

Note that F_0 is not induced by the drive, but is the contribution to F_P arising from the equilibrium quantum/thermal fluctuations in X,

$$F_0 = -\frac{1}{2}X_0^2 = -\frac{1}{2}\frac{E_T(\phi,T)/a^3}{\omega_0^2 + \phi}, \quad E_T(\phi,T) = \hbar\sqrt{\omega_0^2 + \phi}\left[n_b\left(\hbar\sqrt{\omega_0^2 + \phi},\,T\right) + \frac{1}{2}\right] \quad \text{(C4)}$$

where E_T is the energy of the local phonon, a is the lattice constant, n_b is the boson occupation number, and we have restored $\hbar$. At low temperatures $T \ll \omega_0$, the equilibrium contribution to the ponderomotive force in Eq. (C4) is just from the quantum fluctuations (zero point motion) of X. The resulting ponderomotive force/potential is

$$F_0 = -\frac{\hbar}{4a^3}\frac{1}{\sqrt{\omega_0^2 + \phi}}, \quad V_0 = \frac{\hbar}{2a^3}\sqrt{\omega_0^2 + \phi}. \quad \text{(C5)}$$

The drive-induced ponderomotive potential is

$$V_P(\phi) = \frac{E_0^2}{\gamma\omega}\arctan\frac{\gamma\omega}{\omega^2 - \left(\omega_0^2 + \phi\right)}. \quad \text{(C6)}$$

Setting $\phi = g_e\rho$ in Eq. (C6) renders Eq. (11).

a. Estimations for K₃C₆₀

In this section, we make rough estimations of possible light-induced superconductivity in the Fulleride K_3C_{60}. The dimensionless strength of the local density-density interaction is

$$\nu g_P = \nu\frac{\omega^2 - \omega_0^2}{\left[\left(\omega^2 - \omega_0^2\right)^2 + \gamma^2\omega^2\right]^2}g_e^2 E_0^2 = \nu X_{\text{max}}^2\frac{\omega_0^2\gamma^2 - \gamma^4/4}{\left(\omega^2 - \omega_0^2\right)^2 + \gamma^2\omega^2}\frac{\omega^2 - \omega_0^2}{\left(\omega^2 - \omega_0^2\right)^2 + \gamma^2\omega^2}g_e^2 \quad \text{(C7)}$$

where ν is the density states of the electrons at the Fermi energy, and $X_{\text{max}}^2 = \frac{E_0^2}{\omega_0^2\gamma^2 - \gamma^4/4}$ is the maximum mean-square displacement of the phonon that occurs at the frequency $\omega^2 = \omega_0^2 - \gamma^2/2$.

We first estimate X_{max}. Although the pump field E_0 could be very strong, to ensure that the lattice is not destroyed, the maximum possible displacement x of the T_{1u} mode is about $\kappa \sim 0.1$ times the lattice constant a. The corresponding kinetic energy of the local Harmonic oscillator is $K \approx \frac{m_0}{4}\dot{x}^2 \sim \frac{1}{4}m_0\omega_0^2(\kappa a)^2$ where m_0 is the mass of a K_3C_{60} molecule. Since the kinetic energy is also equal to $\frac{1}{2}\omega_0^2 X_{\text{max}}^2 a^3$ according to the continuous field theory in Eq. (C1), we arrive at $X_{\text{max}}^2 \sim m_0\kappa^2/a$.

Now we estimate g_e from Ref. [86] following Ref. [62]. Experimentally [86], the $T_{1u}(1)$ phonon (the lowest T_{1u} mode) of C_{60} with the frequency $\omega_2 = 16\,\text{THz}$ is shifted down by about 2 THz to $\omega_1 = 466\,\text{cm}^{-1} = 14\,\text{THz}$ after being doped to K_6C_{60}. Assuming the downshift is only through the coupling g_e to the doped electrons with density ρ_0, the coupling constant is estimated as $g_e \sim (\omega_2^2 - \omega_1^2)/\rho_0$.

Now Eq. (C7) could be written as

$$\nu g_P \sim \nu\kappa^2\frac{m_0}{a}\frac{\omega_0^2\gamma^2 - \gamma^4/4}{\left(\omega^2 - \omega_0^2\right)^2 + \gamma^2\omega^2}\frac{\omega^2 - \omega_0^2}{\left(\omega^2 - \omega_0^2\right)^2 + \gamma^2\omega^2}\frac{\left(\omega_2^2 - \omega_1^2\right)^2}{\rho_0^2}$$

$$\sim \kappa^2\frac{\omega_0^2\gamma^2 - \gamma^4/4}{\left(\omega^2 - \omega_0^2\right)^2 + \gamma^2\omega^2}\frac{\left(\omega^2 - \omega_0^2\right)\left(\omega_2^2 - \omega_1^2\right)}{\left(\omega^2 - \omega_0^2\right)^2 + \gamma^2\omega^2}\frac{m_0 a^2\left(\omega_2^2 - \omega_1^2\right)}{W}. \quad \text{(C8)}$$

In the second equality we have made use of $\nu \sim \rho_0/W$ where W is the band width, and $\rho_0 \sim 1/a^3$.

The equilibrium contribution g_0 to the local interaction at low temperatures can be found by expanding Eq. (C9) to ρ^2, which gives

$$\nu g_0 = -\frac{\hbar}{16a^3}\frac{\nu g_e^2}{\omega_0^3} = -\frac{\hbar}{16a^3}\frac{\rho_0/W}{\omega_0^3}\frac{\left(\omega_2^2 - \omega_1^2\right)^2}{\rho_0^2} = -\frac{\hbar}{16}\frac{\left(\omega_2^2 - \omega_1^2\right)^2}{W\omega_0^3} \ll 1. \quad \text{(C9)}$$

The black curve in Fig. 3 is plotted as $\nu(g_P + g_0)$ from Eqs. (C8) and (C9) with $\kappa = 0.015$, $\omega_2 = 11\,\text{THz}$, $\omega_1 = 10\,\text{THz}$, $\omega_0 = 10\,\text{THz}$, $\gamma = 2\,\text{THz}$, $W = 1\,\text{eV}$, $a = 1\,\text{nm}$ and $m_0 \approx 1.53 \times 10^6 m_e$. The maximum attraction occurs at about $\omega = \omega_0^2 - \gamma\omega_0$, which yields $|\nu g_P| \sim \kappa^2\frac{\omega_2^2 - \omega_1^2}{\gamma\omega_0}\frac{m_0 a^2(\omega_2^2 - \omega_1^2)}{W} \sim 1$.

b. Light-induced heating

We now estimate the heating effect in a recent pump probe experiment [70] on K_3C_{60}. To show a typical estimate, we pick the experimental parameters at the base temperature of $T_0 = 100$ K (Fig. 3 of Ref. [70]). The pump pulse has the central frequency $\omega = 10$ THz, the duration 1 ps and the fluence $f_E = 0.5$ mJ/cm^2, corresponding to a peak electric field of $E_0 = 1.23 \times 10^4$ V/cm. Assuming the pumped layer is heated up from the base temperature T_0 to a well defined temperature $T_0 + \delta T$, the increase in temperature is estimated as

$$\delta T = \frac{f_E}{C_v d} \approx 1.5 \text{ K} \tag{C10}$$

where C_v is the heat capacity, $d = 2\pi / \text{Im}[\sqrt{\epsilon}\omega/c]$ is the penetration depth of light at the frequency $\omega = 10$ THz, ϵ is the dielectric at this frequency, and c is the speed of light. In Ref. [87], the specific heat of K_3C_{60} is measured to be ≈ 0.2 J/(gK) at 100 K, equivalent to a heat capacity of $C_v \approx 0.39$ J/(cm^{3}K) considering that it has a molar mass of 837 g/mol and a lattice constant of 14.175 Å [70]. The dielectric is $\epsilon = 1 + \frac{4\pi i}{\omega}\sigma(\omega) = -4.4 + 36.0i$ from the optical conductivity $\sigma(\omega) = (200 + 30i)\,\Omega^{-1}\text{cm}^{-1}$ measured at $\omega = 10$ THz {see Fig. 3(b) in Ref. [70]}, giving a penetration depth of $d = 6.6\,\mu$m. If the pulse duration is increased to 4 ps (containing 40 cycles of field oscillation) such that it is convenient to perform a Floquet measurement, the system is heated up by just 6 K.

A similarly estimate for Ta_2NiSe_5 renders $\delta T \approx 16$ K given the same fluence $f_E = 0.5$ mJ/cm^2, the pumping frequency $\omega = 0.2$ eV, the base temperature $T_0 = 150$ K, and the heat capacity and optical properties measured in Ref. [85].

We note that the above estimates are for time regimes after electron-phonon heat transfer (which finishes typically within picoseconds) so that the large heat capacity of the lattice plays a role. Before electron-phonon heat transfer, the injected energy is still in the electronic system, and one may expect the electrons to be much hotter than the estimates. However, not all the energy of the pump is converted into heat. In the clean systems studied in this paper, the energy of the pump is actually converted into collective degrees of freedom, a nonthermal effect that provides the ponderomotive potential.

2. The Raman phonon model

Another example of light-induced e-e attraction is from Raman phonons [78],

$$L = \tfrac{1}{2}\big[-\dot{X}^2 + \omega_0^2(1 + \lambda E(t)^2)X^2 \big] + \rho X \tag{C11}$$

where $E(t)^2 = (E_0\cos\omega t)^2$ couples parametrically to the Raman phonon X either directly or via a IR phonon. Eq. (C11) could be transformed as

$$L = -\frac{1}{2}\dot{X}^2 + \frac{1}{2}\omega_0^2\left[1 + \lambda\frac{1}{2}E_0^2(1 + \cos 2\omega t)\right]X^2 + \rho X = -\frac{1}{2}\dot{X}'^2 + \frac{1}{2}\omega_0'^2 X'^2 - \frac{1}{2\omega_0'^2}\rho^2 + \frac{1}{2}\omega_0^2\lambda\frac{1}{2}E_0^2\cos 2\omega t\left(X' - \frac{\rho}{\omega_0'^2}\right)^2$$

$$= -\frac{1}{2}\dot{X}'^2 + \frac{1}{2}\left(\omega_0'^2 + \frac{1}{4}\omega_0^2\lambda E_0^2\cos 2\omega t\right)X'^2 - \frac{\lambda E_0^2/2}{1 + \lambda E_0^2/2}(\cos 2\omega t)\rho X' - \frac{1}{2\omega_0'^2}\rho^2 \tag{C12}$$

where we defined the shifted phonon frequency $\omega_0'^2 = \omega_0^2(1 + \lambda E_0^2/2)$ and shifted phonon variable $X' = X + \frac{\rho}{\omega_0'^2}$. The electron density ρ is the slow variable and the phonon X is the fast one. At order E_0^4, the $\frac{1}{4}\omega_0^2\lambda E_0^2\cos 2\omega t$ term may contribute to the ponderomotive potential only by the parametric response proportional to quantum/thermal fluctuations, which is small. Therefore, we neglect this term and Eq. (C12) becomes

$$L = \frac{1}{2}\big(-\dot{X}'^2 + \omega_0'^2 X'^2\big) - \frac{\lambda E_0^2/2}{1 + \lambda E_0^2/2}(\cos 2\omega t)\rho X' - \frac{1}{2\omega_0'^2}\rho^2 \tag{C13}$$

where the second term is now the only dynamical driving term. Even with dissipation, Eq. (C13) fits in case 2 in Eq. (4), and the resulting ponderomotive potential is therefore simply obtained from the retarded response function of a Harmonic oscillator as

$$V_P(\rho) = \left[\text{Re}\left[\frac{1}{-4\omega^2 + \omega_0'^2 - i2\gamma\omega}\right]\left(\frac{\lambda E_0^2/2}{1 + \lambda E_0^2/2}\right)^2 - \frac{1}{2\omega_0^2(1 + \lambda E_0^2/2)}\right]\rho^2$$

$$= \frac{1}{2\omega_0^2}\left[-1 + \frac{1}{2}\lambda E_0^2 + \left(-\frac{1}{4} + \text{Re}\left[\frac{\omega_0^2/2}{-4\omega^2 + \omega_0^2 - i2\gamma\omega}\right]\right)\lambda^2 E_0^4 + O(E_0^6)\right]\rho^2. \tag{C14}$$

Equation (C14) is the static component of the effective interaction derived in Ref. [78]. Therefore, there is a positive contribution at order E_0^2, and a negative contribution at order E_0^4 if ω is red tuned relative to ω_0. Since the negative $\lambda^2 E_0^4$ term is resonantly enhanced as ω gets close to ω_0 from the red tuned side, it is possible for it to exceed the positive λE_0^2 contribution, and enhance the attraction interaction.

APPENDIX D: LIGHT-ENGINEERED FREE-ENERGY LANDSCAPE

The Lagrangian for an electronic system exhibiting charge, spin or excitonic order and driven by light $A(t) = A_0(t)\cos\omega t$ is

$$L = \int dr \psi^\dagger \begin{pmatrix} -i\partial_t + \xi(p+A) & \Delta \\ \Delta^* & -i\partial_t - \xi(p+A) \end{pmatrix} \psi + \frac{1}{g}\int dr |\Delta|^2$$

$$= \sum_k (\psi_{ck}^\dagger \quad \psi_{vk}^\dagger)[-i\partial_t + E_k\sigma_3 + \mathbf{A}\cdot\mathbf{j}_k]\begin{pmatrix}\psi_{ck}\\\psi_{vk}\end{pmatrix} + \int dr\left(\frac{1}{g}|\Delta|^2 + \frac{n}{m}A^2\right) \tag{D1}$$

where $\Delta = |\Delta|e^{i\theta}$ is the order parameter. The annihilation operators in the band basis (ψ_{ck}, ψ_{vk}), the "paramagnetic current" $\mathbf{j}_k$, the renormalized quasiparticle energy E_k, and the bare velocity $\mathbf{v}$ are

$$\begin{pmatrix}\psi_{ck}\\\psi_{vk}\end{pmatrix} = \begin{pmatrix}u_k^* & v_k^*\\-v_k & u_k\end{pmatrix}\begin{pmatrix}\psi_{1k}\\\psi_{2k}\end{pmatrix}, \quad (u_k, v_k) = \frac{1}{\sqrt{2}}\left(\sqrt{1+\frac{\xi_k}{E_k}}, \; e^{i\theta}\sqrt{1-\frac{\xi_k}{E_k}}\right)$$

$$\mathbf{j}_k = \frac{\mathbf{v}_k}{E_k}\begin{pmatrix}\xi_k & \Delta\\\Delta^* & -\xi_k\end{pmatrix}, \quad E_k = \sqrt{\xi_k^2 + \Delta^2}, \quad \mathbf{v}_k = \partial_\mathbf{k}\xi_k. \tag{D2}$$

To obtain the ponderomotive force F_P for the order parameter Δ, we integrate out the fermions ψ in the Keldysh path integral and look for $O(\Delta_q)$ terms in the resulting action, as indicated by Eq. (A3). Without losing important information, we focus on the force on the amplitude direction and take Δ to be real. Δ enters the driven fermions in two places: the periodic driving term $\mathbf{A}\cdot\mathbf{j}$, and the quasiparticle energy E_k. Taking a partial derivative with respect to Δ, one obtains the force operator,

$$\hat{F}_P = \hat{F}_1 + \hat{F}_2, \quad \hat{F}_1 = \sum_k \mathbf{A}\cdot\mathbf{v}_k(\psi_{ck}^\dagger \quad \psi_{vk}^\dagger)\left[\partial_\Delta\begin{pmatrix}\frac{\xi_k}{E_k} & \frac{\Delta}{E_k}\\\frac{\Delta}{E_k} & -\frac{\xi_k}{E_k}\end{pmatrix}\right]\begin{pmatrix}\psi_{ck}\\\psi_{vk}\end{pmatrix}, \quad \hat{F}_2 = \sum_k \partial_\Delta E_k(\psi_{ck}^\dagger \quad \psi_{vk}^\dagger)\sigma_3\begin{pmatrix}\psi_{ck}\\\psi_{vk}\end{pmatrix}. \tag{D3}$$

The ponderomotive force $F_\text{P} = F_1 + F_2$ is the path integral average of $\hat{F}_P$.

In this paper, we compute F_P only at order $A_0^2 = E_0^2/\omega^2$. At this order, the $\hat{F}_1$ term contributes only by two-point correlators of $\mathbf{j}$, which has contributions only from the interband terms $\mathbf{v}_k\frac{\Delta}{E_k}(\psi_{ck}^\dagger\psi_{vk} + \text{c.c.})$. The corresponding ponderomotive force is found simply from the retarded two-point correlation function,

$$F_1 = A_0^2\int dt e^{i\omega t}\langle j_q(t)F_{1c}(0)\rangle = A_0^2\sum_k v_{xk}^2\frac{\Delta}{E_k}\left(\partial_\Delta\frac{\Delta}{E_k}\right)\sum_\Omega \text{Tr}[\hat{G}_k(\Omega)\hat{\gamma}_1\hat{\gamma}_c\hat{G}_k(\Omega+\omega)\hat{\gamma}_j\hat{\gamma}_q]$$

$$= A_0^2\sum_k v_{xk}^2\frac{\Delta}{E_k}\left(\partial_\Delta\frac{\Delta}{E_k}\right)\text{Re}\left[\frac{-8E_k}{(\omega+i\gamma)^2 - 4E_k^2}\right] = -A_0^2\frac{v_F^2}{d}v\frac{4}{\Delta}\int d\xi\frac{2\Delta^2\xi^2}{E^3}\text{Re}\left[\frac{1}{(\omega+i\gamma)^2 - 4E^2}\right]$$

$$\equiv -A_0^2\frac{v_F^2}{d}\frac{4}{\Delta}v f_1\left(\frac{\Delta}{\omega}, \frac{\gamma}{\omega}\right) \tag{D4}$$

where F_{1c} and j_q are the "classical" and "quantum" components [43,44] of these operators defined in the same way as those below Eq. (A1), $E = \sqrt{\Delta^2 + \xi^2}$, γ is the quasiparticle damping rate, d is the space dimension, and ν is the density of states at the Fermi energy before the gap opening. The $\hat{\gamma}_c = \tau_0\sigma_0$, $\hat{\gamma}_q = \tau_1\sigma_0$, $\hat{\gamma}_j = \tau_0\sigma_1$, $\hat{\gamma}_1 = \tau_0\sigma_1$ are the vertices for the classical source, quantum source, the current, and the force F_1. The 4×4 Green's function

$$\hat{G}_k(\omega) = -i\langle\psi\bar{\psi}\rangle|_\omega$$

$$= \begin{pmatrix}G_k^R(\omega) & G_k^K(\omega)\\0 & G_k^A(\omega)\end{pmatrix} = \begin{pmatrix}(\omega+i\gamma - E_k\sigma_3)^{-1} & (G_k^R(\omega) - G_k^A(\omega))\tanh\frac{\omega}{2T}\\0 & (\omega-i\gamma - E_k\sigma_3)^{-1}\end{pmatrix} \tag{D5}$$

is in the Keldysh notation and in the band basis.

The $\hat{F}_2$ term contributes to the force by three-point correlators,

$$F_2 = A_0^2\int dt_1 dt_2 e^{i\omega(t_1-t_2)}\langle j_q(t_1)j_q(t_2)F_{2c}(0)\rangle = A_0^2\sum_k\left(v_{xk}\frac{\Delta}{E_k}\right)^2(\partial_\Delta E_k)\sum_\Omega\text{Tr}[\hat{G}(\Omega)\hat{\gamma}_c\hat{\gamma}_j\hat{G}(\Omega+\omega)\hat{\gamma}_c\hat{\gamma}_j\hat{G}(\Omega)\hat{\gamma}_q\hat{\gamma}_2]$$

$$= A_0^2\sum_k\left(v_{xk}\frac{\Delta}{E_k}\right)^2(\partial_\Delta E_k)\sum_\Omega\text{Tr}[G_k^R(\Omega)G_k^K(\Omega)G_k^R(\Omega+\omega) + G_k^R(\Omega)G_k^A(\Omega)G_k^K(\Omega+\omega) + G_k^K(\Omega)G_k^A(\Omega)G_k^A(\Omega+\omega)]$$

$$= A_0^2\sum_k\left(v_{xk}\frac{\Delta}{E_k}\right)^2(\partial_\Delta E_k)\frac{2}{3}\left(\frac{2\tanh\left(\frac{-E_k}{T}\right) - \tanh\left(\frac{E_k}{T}\right)}{(\omega - 2E_k)^2 + \gamma^2} + \frac{\tanh\left(\frac{-E_k}{T}\right) - 2\tanh\left(\frac{E_k}{T}\right)}{(\omega + 2E_k)^2 + \gamma^2}\right)$$
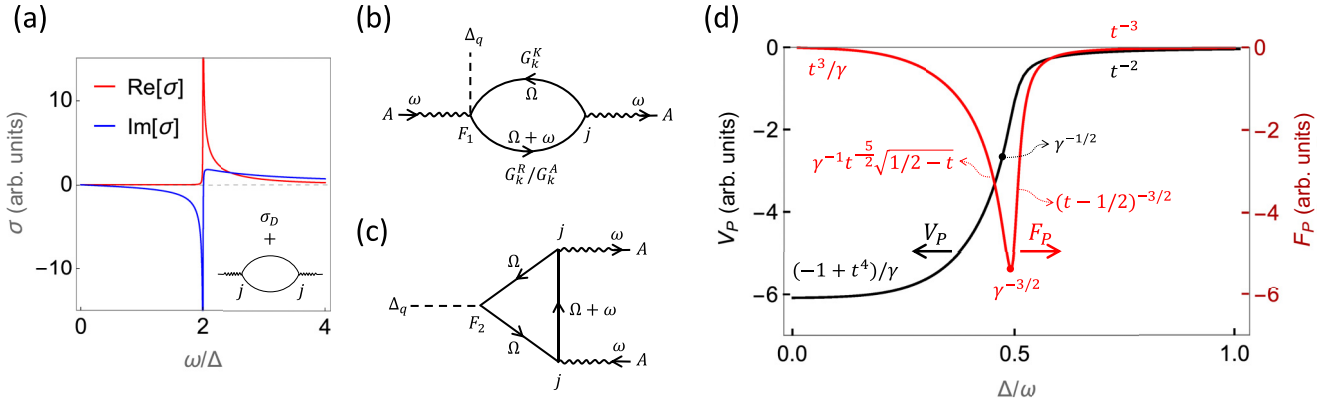
FIG. 6. (a) The optical conductivity of an electronic system with charge/spin/excitonic order in the BCS weak coupling case. Inset is the contributions to the optical conductivity: the diamagnetic part $\sigma_D = ine^2/(m\omega)$ plus the current-current correlation. (b)(c) The Feynman diagram representing the F_1/F_2 part of the ponderomotive force. (d) Red curve is the ponderomotive force $F_P(\Delta)$ as a function of Δ/ω for a quasiparticle damping rate of $\gamma = 0.03$ in units of ω. Black curve is the corresponding ponderomotive potential. The inset expressions are their asymptotic behaviors in each region, with $t = \Delta/\omega$, γ in units of ω, and the colors matching the curves they refer to.

$$\xrightarrow{T=0} A_0^2 \sum_k \left(v_{xk} \frac{\Delta}{E_k} \right)^2 (\partial_\Delta E_k) \left[-2 \left(\frac{1}{(\omega - 2E_k)^2 + \gamma^2} + \frac{1}{(\omega + 2E_k)^2 + \gamma^2} \right) \right]$$

$$= -A_0^2 \frac{v_F^2}{d} \frac{4}{\Delta} v \int d\xi \frac{\Delta^4}{2E^3} \left(\frac{1}{(\omega - 2E)^2 + \gamma^2} + \frac{1}{(\omega + 2E)^2 + \gamma^2} \right) \equiv -A_0^2 \frac{v_F^2}{d} \frac{4}{\Delta} v f_2 \left(\frac{\Delta}{\omega}, \frac{\gamma}{\omega} \right) \tag{D6}$$

where $\hat{\gamma}_2 = \tau_0 \sigma_3$.

From Eq. (D6), it is seen that each quasiparticle excitation (may also be viewed as the resonant excitation of a two-level system) contributes a pole $1/((\omega - 2E)^2 + \gamma^2)$ to F_P whose spectra weight scales as $1/\gamma$. This is a canonical example of the dissipative contribution to the ponderomotive force when the slow field enters by shifting the energy $2E$ of a two-level system.

The total ponderomotive force is therefore

$$F_P = A_0^2 \sum_k v_{xk}^2 \left\{ \frac{\Delta}{E_k} \left(\partial_\Delta \frac{\Delta}{E_k} \right) \text{Re} \left[\frac{-8E_k}{(\omega + i\gamma)^2 - 4E_k^2} \right] + 2 \frac{\Delta^2 \partial_\Delta E_k}{E_k^2} \left[\frac{-1}{(\omega - 2E_k)^2 + \gamma^2} + (E_k \to -E_k) \right] \right\}$$

$$= F_1 + F_2 = -A_0^2 \frac{v_F^2}{d} v \frac{4}{\Delta} \left[f_1 \left(\frac{\Delta}{\omega}, \frac{\gamma}{\omega} \right) + f_2 \left(\frac{\Delta}{\omega}, \frac{\gamma}{\omega} \right) \right] \tag{D7}$$

and the ponderomotive potential is

$$V_P = -\int F_P d\Delta = V_u(E_0, \omega) g_P \left(\frac{\Delta}{\omega}, \frac{\gamma}{\omega} \right), \quad V_u = \frac{v\omega^2}{d} \left(\frac{eE_0}{\omega^2/v_F} \right)^2, \quad g_P(t, \delta) = \int_\infty^t dx \frac{4}{x} [f_1(x, \delta) + f_2(x, \delta)] \tag{D8}$$

where V_u is a scale of energy density determined by the driving field E_0 and frequency ω, and g_P, f_1, f_2 are dimensionless functions of Δ/ω and γ/ω only.

In Fig. 6(d), we plot the dimensionless F_P and V_P. The negative sign of F_P means that it always tends to push Δ to smaller values. As Δ decreases to around $\omega/2$, there is a strong peak in F_P because of the quasiparticle excitations [see also the optical conductivity in Fig. 6(a)], which results in a sharp drop of V_P to its value $\sim -1/\gamma$ at $\Delta = 0$. This combined with the equilibrium contribution to the free energy F_0 results in the new free energy minimum in $F_0 + V_P$, see Fig. 4. We also show the asymptotic values of F_P and V_P in different regimes of Fig. 6, which gives the schematic phase diagram in the inset of Fig. 4.

We note that in principle, in the resonance regime $2\Delta < \omega$, the expansion of V_P at the order of E_0^2 is a good approximation when $\kappa = eE_0 v_F/(\omega\gamma) \ll 1$. To obtain the corrections at large fields, one may employ the exact solutions for the driven-dissipative two levels system, one for each Anderson-pseudo spin. We leave it for future study.

Insights from the optical conductivity

One may check that in the dissipationless limit, meaning $\gamma \to 0$ and $\omega < 2\Delta$, the ponderomotive potential [Eq. (D7)] reduces to that predicted by Lemma 1,

$$V_P = \text{Re} \left[-\frac{i}{\omega} \sigma(\Delta, \omega) \right] E_0^2. \tag{D9}$$

where σ may be found from Eq. (12) of Ref. [84], also shown in Fig. 6(a). According to Eq. (D9), the behavior of V_P at $\Delta > \omega/2$ [black curve in Fig. 6(d)] may be understood from the sub-gap optical conductivity [blue curve at $\omega < 2\Delta$ in Fig. 6(a)]. Giving a driving frequency $\omega < 2\Delta$, it is obvious that if the gap decreases, the V_P in Eq. (D9) would drop.

Equation (D9) also explains the light tuned competing superconducting and charge orders in the attractive Hubbard model discussed by Sentef *et al.* [30]. If the spectra weight shift because of the phase mode is ignored as in Ref. [30], the CDW state has an optical conductivity shown in Fig. 6(a), while the superconducting state has no optical absorptions [$\sigma = ine^2/(m\omega)$]. When driven with a subgap frequency $\omega < 2\Delta$, the CDW state gains a negative V_P while the superconducting state has a positive V_P, as shown by Eq. (D9). Therefore, the drive favors the CDW state. When driven with a frequency right above the gap, assuming Eq. (D9) still works, the V_P of the CDW state jumps to the a positive value, and may instead favor the superconducting state.

---

[1] L. M. Sieberer, M. Buchhold, and S. Diehl, Keldysh field theory for driven open quantum systems, Rep. Prog. Phys. **79**, 096001 (2016).

[2] D. N. Basov, R. D. Averitt, and D. Hsieh, Towards properties on demand in quantum materials, Nat. Mater. **16**, 1077 (2017).

[3] A. Eckardt, Colloquium: Atomic quantum gases in periodically driven optical lattices, Rev. Mod. Phys. **89**, 011004 (2017).

[4] M. S. Rudner and N. H. Lindner, Band structure engineering and non-equilibrium dynamics in Floquet topological insulators, Nat. Rev. Phys. **2**, 229 (2020).

[5] A. de la Torre, D. M. Kennes, M. Claassen, S. Gerber, J. W. McIver, and M. A. Sentef, Colloquium: Nonthermal pathways to ultrafast control in quantum materials, Rev. Mod. Phys. **93**, 041002 (2021).

[6] C. Bao, P. Tang, D. Sun, and S. Zhou, Light-induced emergent phenomena in 2D materials and topological materials, Nat. Rev. Phys. **4**, 33 (2022).

[7] W. W. Ho, T. Mori, D. A. Abanin, and E. G. Dalla Torre, Quantum and classical Floquet prethermalization, Ann. Phys. (NY) **454**, 169297 (2023).

[8] Y. Murakami, D. Goležˇ, M. Eckstein, and P. Werner, Photo-induced nonequilibrium states in Mott insulators, arXiv:2310.05201.

[9] L. M. Sieberer, M. Buchhold, J. Marino, and S. Diehl, Universality in driven open quantum matter, arXiv:2312.03073.

[10] T. Mori, Floquet states in open quantum systems, Annu. Rev. Condens. Matter Phys. **14**, 35 (2023).

[11] F. Mahmood, C.-K. Chan, Z. Alpichshev, D. Gardner, Y. Lee, P. A. Lee, and N. Gedik, Selective scattering between Floquet–Bloch and Volkov states in a topological insulator, Nat. Phys. **12**, 306 (2016).

[12] J. W. McIver, B. Schulte, F. U. Stein, T. Matsuyama, G. Jotzu, G. Meier, and A. Cavalleri, Light-induced anomalous Hall effect in graphene, Nat. Phys. **16**, 38 (2020).

[13] J.-Y. Shan, M. Ye, H. Chu, S. Lee, J.-G. Park, L. Balents, and D. Hsieh, Giant modulation of optical nonlinearity by Floquet engineering, Nature (London) **600**, 235 (2021).

[14] S. Zhou, C. Bao, B. Fan, H. Zhou, Q. Gao, H. Zhong, T. Lin, H. Liu, P. Yu, P. Tang *et al.*, Pseudospin-selective Floquet band engineering in black phosphorus, Nature (London) **614**, 75 (2023).

[15] N. H. Lindner, G. Refael, and V. Galitski, Floquet topological insulator in semiconductor quantum wells, Nat. Phys. **7**, 490 (2011).

[16] M. Bukov, L. D'Alessio, and A. Polkovnikov, Universal high-frequency behavior of periodically driven systems: From dynamical stabilization to Floquet engineering, Adv. Phys. **64**, 139 (2015).

[17] R. Moessner and S. L. Sondhi, Equilibration and order in quantum Floquet matter, Nat. Phys. **13**, 424 (2017).

[18] T. Oka and S. Kitamura, Floquet engineering of quantum materials, Annu. Rev. Condens. Matter Phys. **10**, 387 (2019).

[19] S. Ito, M. Schüler, M. Meierhofer, S. Schlauderer, J. Freudenstein, J. Reimann, D. Afanasiev, K. A. Kokh, O. E. Tereshchenko, J. Güdde, M. A. Sentef, U. Höfer, and R. Huber, Build-up and dephasing of FloquetBloch bands on subcycle timescales, Nature **616**, 696 (2023).

[20] T. Oka and H. Aoki, Photovoltaic Hall effect in graphene, Phys. Rev. B **79**, 081406(R) (2009).

[21] T. Kitagawa, E. Berg, M. Rudner, and E. Demler, Topological characterization of periodically driven quantum systems, Phys. Rev. B **82**, 235114 (2010).

[22] K. I. Seetharam, C.-E. Bardyn, N. H. Lindner, M. S. Rudner, and G. Refael, Controlled population of Floquet-Bloch states via coupling to Bose and Fermi baths, Phys. Rev. X **5**, 041050 (2015).

[23] L. He, Z. Addison, J. Jin, E. J. Mele, S. G. Johnson, and B. Zhen, Floquet Chern insulators of light, Nat. Commun. **10**, 4194 (2019).

[24] Z. Yang, Q. Yang, J. Hu, and D. E. Liu, Dissipative Floquet Majorana modes in proximity-induced topological superconductors, Phys. Rev. Lett. **126**, 086801 (2021).

[25] N. Goldman and J. Dalibard, Periodically driven quantum systems: Effective Hamiltonians and engineered gauge fields, Phys. Rev. X **4**, 031027 (2014).

[26] T. Kuwahara, T. Mori, and K. Saito, Floquet–Magnus theory and generic transient dynamics in periodically driven many-body quantum systems, Ann. Phys. (NY) **367**, 96 (2016).

[27] D. A. Abanin, W. De Roeck, W. W. Ho, and F. Huveneers, Effective Hamiltonians, prethermalization, and slow energy absorption in periodically driven many-body systems, Phys. Rev. B **95**, 014112 (2017).

[28] M. Claassen, H.-C. Jiang, B. Moritz, and T. P. Devereaux, Dynamical time-reversal symmetry breaking and photo-induced chiral spin liquids in frustrated Mott insulators, Nat. Commun. **8**, 1192 (2017).

[29] Y. Wan and R. Moessner, Control of the effective free-energy landscape in a frustrated magnet by a field pulse, Phys. Rev. Lett. **119**, 167203 (2017).

[30] M. A. Sentef, A. Tokuno, A. Georges, and C. Kollath, Theory of laser-controlled competing superconducting and charge orders, Phys. Rev. Lett. **118**, 087002 (2017).

[31] M. Schüler, D. Golež, Y. Murakami, N. Bittner, A. Herrmann, H. U. Strand, P. Werner, and M. Eckstein, Nessi: The non-equilibrium systems simulation package, Comput. Phys. Commun. **257**, 107484 (2020).

[32] C. Xie, A. D. Smith, H. Yan, W.-C. Chen, and Y. Wang, Dynamical approach to realize room-temperature superconductivity in LaH_{10}, arXiv:2312.12706.

[33] L. Berthier, L. F. Cugliandolo, and J. L. Iguain, Glassy systems under time-dependent driving forces: Application to slow granular rheology, Phys. Rev. E **63**, 051302 (2001).

[34] Y. M. Aliev, V. Y. Bychenkov, A. A. Frolov, and M. S. Jovanović, The kinetic theory of the nonlinear low-frequency response of a collisionless plasma to high-frequency electromagnetic radiation, J. Plasma Phys. **48**, 167 (1992).

[35] Z. Sun, D. N. Basov, and M. M. Fogler, Universal linear and nonlinear electrodynamics of a Dirac fluid, Proc. Natl. Acad. Sci. USA **115**, 3285 (2018).

[36] C. Wolff, C. Tserkezis, and N. A. Mortensen, Enhanced ponderomotive force in graphene due to interband resonance, New J. Phys. **21**, 073046 (2019).

[37] A. Rikhter, D. N. Basov, and M. M. Fogler, Modeling of plasmonic and polaritonic effects in photocurrent nanoscopy, J. Appl. Phys. **135**, 103101 (2024).

[38] P. Kapitza, Dynamic stability of the pendulum with vibrating suspension point, Sov. Phys. JETP **21**, 588 (1951).

[39] R. Grimm, M. Weidemüller, and Y. B. Ovchinnikov, Optical dipole traps for neutral atoms, Adv. At. Mol. Opt. Phys. **42**, 95 (2000).

[40] J. R. Moffitt, Y. R. Chemla, S. B. Smith, and C. Bustamante, Recent advances in optical tweezers, Annu. Rev. Biochem. **77**, 205 (2008).

[41] L. P. Kadanoff and G. Baym, *Quantum Statistical Mechanics: Green's Function Methods in Equilibrium and Nonequilibrium Problems* (W.A. Benjamin, New York, 1962).

[42] L. V. Keldysh, Diagram technique for nonequilibrium processes, Zh. Eksp. Teor. Fiz. **47**, 1515 (1964).

[43] A. Kamenev, *Field Theory of Non-Equilibrium Systems* (Cambridge University Press, Cambridge, 2011).

[44] A. Altland and B. D. Simons, *Condensed Matter Field Theory* (Cambridge University Press, Cambridge, 2010).

[45] R. W. Boyd, *Nonlinear Optics*, 3rd ed. (Academic Press, Boca Raton, FL, 2008).

[46] T. Shirai, J. Thingna, T. Mori, S. Denisov, P. Hänggi, and S. Miyashita, Effective Floquet–Gibbs states for dissipative quantum systems, New J. Phys. **18**, 053008 (2016).

[47] T. N. Ikeda and M. Sato, General description for nonequilibrium steady states in periodically driven dissipative quantum systems, Sci. Adv. **6**, eabb4019 (2020).

[48] H. Dehghani, T. Oka, and A. Mitra, Dissipative Floquet topological systems, Phys. Rev. B **90**, 195429 (2014).

[49] F. Song, S. Yao, and Z. Wang, Non-Hermitian skin effect and chiral damping in open quantum systems, Phys. Rev. Lett. **123**, 170401 (2019).

[50] A. Mitra, I. Aleiner, and A. J. Millis, Semiclassical analysis of the nonequilibrium local polaron, Phys. Rev. Lett. **94**, 076404 (2005).

[51] A. Mitra, S. Takei, Y. B. Kim, and A. J. Millis, Nonequilibrium quantum criticality in open electronic systems, Phys. Rev. Lett. **97**, 236808 (2006).

[52] M. Bukov, M. Kolodrubetz, and A. Polkovnikov, Schrieffer-Wolff transformation for periodically driven systems: Strongly correlated systems with artificial gauge fields, Phys. Rev. Lett. **116**, 125301 (2016).

[53] Z. Sun, D. N. Basov, and M. M. Fogler, Third-order optical conductivity of an electron fluid, Phys. Rev. B **97**, 075432 (2018).

[54] Z. Sun, Y. Murakami, T. Kaneko, D. Golež, and A. J. Millis, Dynamical exciton condensates in biased electron-hole bilayers, arXiv:2312.06426.

[55] N. F. Mott, The transition to the metallic state, Philos. Mag. **6**, 287 (1961).

[56] M. M. Fogler, L. V. Butov, and K. S. Novoselov, High-temperature superfluidity with indirect excitons in van der Waals heterostructures, Nat. Commun. **5**, 4555 (2014).

[57] E. Perfetto and G. Stefanucci, Floquet topological phase of nondriven *p*-wave nonequilibrium excitonic insulators, Phys. Rev. Lett. **125**, 106401 (2020).

[58] L. V. Butov, A. Zrenner, G. Abstreiter, G. Böhm, and G. Weimann, Condensation of indirect excitons in coupled AlAs/GaAs quantum Wells, Phys. Rev. Lett. **73**, 304 (1994).

[59] L. Ma, P. X. Nguyen, Z. Wang, Y. Zeng, K. Watanabe, T. Taniguchi, A. H. MacDonald, K. F. Mak, and J. Shan, Strongly correlated excitonic insulator in atomic double layers, Nature (London) **598**, 585 (2021).

[60] R. Wang, T. A. Sedrakyan, B. Wang, L. Du, and R.-R. Du, Excitonic topological order in imbalanced electron–hole bilayers, Nature (London) **619**, 57 (2023).

[61] D. Fröhlich, A. Nöthe, and K. Reimann, Observation of the resonant optical Stark effect in a semiconductor, Phys. Rev. Lett. **55**, 1335 (1985).

[62] D. M. Kennes, E. Y. Wilner, D. R. Reichman, and A. J. Millis, Transient superconductivity from electronic squeezing of optically pumped phonons, Nat. Phys. **13**, 479 (2017).

[63] M. A. Sentef, Light-enhanced electron-phonon coupling from nonlinear electron-phonon coupling, Phys. Rev. B **95**, 205111 (2017).

[64] A. Grankin, M. Hafezi, and V. M. Galitski, Enhancement of superconductivity with external phonon squeezing, Phys. Rev. B **104**, L220503 (2021).

[65] C. J. Eckhardt, S. Chattopadhyay, D. M. Kennes, E. A. Demler, M. A. Sentef, and M. H. Michael, Theory of resonantly enhanced photo-induced superconductivity, Nat. Commun. **15**, 2300 (2024).

[66] K. Kovač, D. Golež, M. Mierzejewski, and J. Bonča, Optical manipulation of bipolarons in a system with nonlinear electron-phonon coupling, Phys. Rev. Lett. **132**, 106001 (2024).

[67] M. Yarmohammadi, M. Bukov, and M. H. Kolodrubetz, Nonequilibrium phononic first-order phase transition in a driven fermion chain, Phys. Rev. B **108**, L140305 (2023).

[68] R. Shankar, Renormalization-group approach to interacting fermions, Rev. Mod. Phys. **66**, 129 (1994).

[69] H. Gao, F. Schlawin, M. Buzzi, A. Cavalleri, and D. Jaksch, Photoinduced electron pairing in a driven cavity, Phys. Rev. Lett. **125**, 053602 (2020).

[70] E. Rowe, B. Yuan, M. Buzzi, G. Jotzu, Y. Zhu, M. Fechner, M. Först, B. Liu, D. Pontiroli, M. Riccò, and A. Cavalleri, Resonant enhancement of photo-induced superconductivity in K_3C_{60}, Nat. Phys. **19**, 1821 (2023).

[71] M. Buzzi, G. Jotzu, A. Cavalleri, J. I. Cirac, E. A. Demler, B. I. Halperin, M. D. Lukin, T. Shi, Y. Wang, and D. Podolsky, Higgs-mediated optical amplification in a nonequilibrium superconductor, Phys. Rev. X **11**, 011055 (2021).

[72] D. van der Marel, F. Barantani, and C. W. Rischau, Possible mechanism for superconductivity in doped $SrTiO_3$, Phys. Rev. Res. **1**, 013003 (2019).

[73] M. Mitrano, A. Cantaluppi, D. Nicoletti, S. Kaiser, A. Perucchi, S. Lupi, P. Di Pietro, D. Pontiroli, M. Riccó, S. R. Clark *et al.*, Possible light-induced superconductivity in K_3C_{60} at high temperature, Nature (London) **530**, 461 (2016).

[74] A. Cantaluppi, M. Buzzi, G. Jotzu, D. Nicoletti, M. Mitrano, D. Pontiroli, M. Riccó, A. Perucchi, P. Di Pietro, and A. Cavalleri, Pressure tuning of light-induced superconductivity in K_3C_{60}, Nat. Phys. **14**, 837 (2018).

[75] M. Budden, T. Gebert, M. Buzzi, G. Jotzu, E. Wang, T. Matsuyama, G. Meier, Y. Laplace, D. Pontiroli, M. Riccó *et al.*, Evidence for metastable photo-induced superconductivity in K_3C_{60}, Nat. Phys. **17**, 611 (2021).

[76] S. Chattopadhyay, C. J. Eckhardt, D. M. Kennes, M. A. Sentef, D. Shin, A. Rubio, A. Cavalleri, E. A. Demler, and M. H. Michael, Mechanisms for long-lived, photo-induced superconductivity, arXiv:2303.15355.

[77] Z. Sun and A. J. Millis, Transient trapping into metastable states in systems with competing orders, Phys. Rev. X **10**, 021028 (2020).

[78] M. Babadi, M. Knap, I. Martin, G. Refael, and E. Demler, Theory of parametrically amplified electron-phonon superconductivity, Phys. Rev. B **96**, 014512 (2017).

[79] Y. Murakami, N. Tsuji, M. Eckstein, and P. Werner, Nonequilibrium steady states and transient dynamics of conventional superconductors under phonon driving, Phys. Rev. B **96**, 045125 (2017).

[80] D. Jérome, T. M. Rice, and W. Kohn, Excitonic insulator, Phys. Rev. **158**, 462 (1967).

[81] G. Grüner, The dynamics of charge-density waves, Rev. Mod. Phys. **60**, 1129 (1988).

[82] G. Grüner, The dynamics of spin-density waves, Rev. Mod. Phys. **66**, 1 (1994).

[83] Z. Sun and A. J. Millis, Topological charge pumping in excitonic insulators, Phys. Rev. Lett. **126**, 027601 (2021).

[84] Z. Sun and A. J. Millis, Bardasis-schrieffer polaritons in excitonic insulators, Phys. Rev. B **102**, 041110(R) (2020).

[85] Y. F. Lu, H. Kono, T. I. Larkin, A. W. Rost, T. Takayama, A. V. Boris, B. Keimer, and H. Takagi, Zero-gap semiconductor to excitonic insulator transition in Ta_2NiSe_5, Nat. Commun. **8**, 14408 (2017).

[86] P. Giannozzi and W. Andreoni, Effects of doping on the vibrational properties of C_{60} from first principles: K_6C_{60}, Phys. Rev. Lett. **76**, 4915 (1996).

[87] K. Allen and F. Hellman, Specific heat of C_{60} and K_3C_{60} thin films for $t = 6$–400 k, Phys. Rev. B **60**, 11765 (1999).